Rainfall erosivity mapping over mainland China based on high density hourly rainfall records

Tianyu Yue[1], Shuiqing Yin[1], Yun Xie[1], Bofu Yu[2], Baoyuan Liu[1]

[1]State Key Laboratory of Earth Surface Processes and Resource Ecology, Faculty of Geographical Science, Beijing Normal University, Beijing, 100875, China
[2]Australian Rivers Institute, School of Engineering and Built Environment, Griffith University, Nathan, Queensland, QLD 4111, Australia

Correspondence to: Shuiqing Yin (yinshuiqing@bnu.edu.cn)

Abstract. Rainfall erosivity represents the effect of rainfall and runoff on the average rate of soil losserosion. Maps of rainfall erosivity are necessary indispensable for soil erosion assessment and sediment transportation estimation based on using the Universal Soil Loss Equation (USLE) and its successors. To improve currently available erosivity maps based on daily rainfall data from 774 stations for mainland China, hourly and daily rainfall data from 2,381 stations for the period 1951-2018 were collected to generate the R factorR-factor and the 1-in-10-year EI_{30} maps (available at https://dx.doi.org/10.12275/bnu.clicia.rainfallerosivity.CN.001; Yue et al., 2020). RIndependent Rrainfall data at 1-min intervals from 62 stations, of which (18 stations with data lengths greatermore than 29 years of data,) were usedcollected to calculate rainfall erosivities as true values to evaluate the accuracy improvement of the new R factorR-factor and map (1-in-10-year EI_{30} maps) as well asnd the improvements from the current maps based through on a cross-validation process. The results showed that: (1) cBoth the R factorR-factor and 1-in-10-year EI_{30} decreased from the southeastern to the northwestern, ranging from 0 to 25,300 MJ mm ha^{-1} h^{-1} a^{-1} for the R factorR-factor and 0 to 11,246 MJ mm ha^{-1} h^{-1} for the 1-in-10-year EI_{30}. New maps indicated Ccurrent maps existed an underestimated erosivity ion forfor most of the south-eastern part of China areas areas and an overestimatedion for most of the middle and western regionareas.; (2) tThe R-factor map generated in this study had a median absolute relative error of 16% for the western region, and 17.8% for the rest of Chinamid-western and eastern regions, and 16.2% for the western region, and the 1-in-10-year EI_{30} map had median absolute relative error of 13.54%, expceept for for the mid-western and eastern regions, whereas no evaluation for the western region for which no evaluation was made because of data limitationdue to short data lengths for stations with 1-min rainfall observations in western region; (3) cComparing with the current maps, the improvement inof the R-factor map generated in this study occurredwas mainly in the western regions, anddecreasing the median absolute relative error was reduced from 1621.6% to 16.2%, because of anmainly due to the increase in theof the number of stations from 87 to 150 stations and anthe increased of the data temporal resolution from daily data to hourly data. The map of 1-in-10-year EI_{30} in this study improved the accuracy from 20.6% to 13.5% for the middle and east of China western and eastern regions; Comparing with the current maps, the R factorR-factor map generated in this study improved the accuracy from 19.48.1% to 15.97.8% in the mid-western and eastern regions, from 45.2161.6% to 21.616.2% in the western region, and the 1-in-10-year EI_{30} map in the mid-western and eastern regions

~~improved the accuracy from 21.70.6% to 13.05%. The improvement of the new R factor~~R-factor map can be mainly ~~contributed to the increase of data resolution from daily data to hourly data, whereas that of new 1-in-10-year EI_{30} map to the~~ ~~increase of the number of stations, especially in weastern regions (from 87 to 150) from 744 to 2381. (4)~~ the benefit of increased ~~The effect of increasing the number of~~ station density for erosivity mapping is limited ~~s to improve the interpolation of R-factor and 1-in-10-year EI_{30} seems to be not very obvious~~ when the station density reached ~~was denser than~~ about ~~10-103 km2~~ 1 station per~~every~~ 10,000 km^2.

1 Introduction

Soil erosion has been the major threat to soil health, soil and river ecosystem services in many regions of the world (FAO, 2019b). Soil erosion has on-site impacts, such as the reduction of soil and water, the loss of soil nutrients, the decrease of land quality and food production, as well as off-site impacts, such as excessive sedimentation and water pollution~~. The reduction of crop production due to erosion has been estimated to be 0.4% per year on a global scale (FAO, 2019b)~~.

Soil erosion models are tools to evaluate the rate of soil loss and can provide policymakers useful information for taking measures in soil and water conservation. The Universal Soil Loss Equation (USLE; Wischmeier and Smith, 1965, 1978) and the Revised USLE (RUSLE; Renard, 1997; USDA-ARS, 2013) have been widely used to estimate soil erosion in at least 109 countries over the past 40 years (Alewell et al., 2019). Rainfall erosivity is one of the factors in the USLE and RUSLE to represent the potential ability of rainfall and runoff to affect soil erosion.

In the USLE, erosivity of a rainfall event is identified as the EI value, also denoted as EI_{30}, which is the product of the total storm energy (E) and the maximum 30-min intensity (I_{30}) (Wischmeier, 1959). The erosivity factor (~~R factor~~R-factor) in the USLE is the average annual total EI values of all erosive events. To recognize interannual rainfall variability, rainfall data of long periods are required (Wischmeier and Smith, 1978). In the original isoerodent map generated by Wischmeier and Smith (1965), stations with rainfall data of at least 22 years were used.

To use the USLE, two additional input parameters are required. One is the seasonal distribution of the ~~R factor~~R-factor. To acquire soil erodibility factor (K factor) and cover-management factor (C factor), the seasonal distribution of EI (monthly, Wischmeier and Smith, 1965; or half-month percentage of EI, Renard, 1997, Wischmeier and Smith, 1978) were needed. The other is the 1-in-10-year storm EI value needed to compute the support practice factor (P factor) for the contour farming (Renard, 1997).

~~Calculation of the rainfall erosivity factor requires high-resolution rainfall data to compute E and I_{30} accurately.~~ Kinetic energy generated by raindrops can be calculated based on raindrop disdrometer data and estimated based on breakpoint or hyetograph data via KE-I equations, while I_{30} is expected to be prepared using breakpoint or hyetograph data with an observed interval ≤ 30 min. In the original study of event rainfall erosivity, the recording-rain-gauge chart was used (Wischmeier and Smith, 1958). However, these data were usually in shortage not only in the length but also in the spatial coverage~~Meteorological stations with this type of data are sparsely distributed and the record length is usually quite short~~.

Methods to estimate rainfall erosivity based on more readily available data have been developed widely, such as daily (Angulomartínez and Beguería, 2009; Bagarello and D'Asaro, 1994; Capolongo et al., 2008; Haith and Merrill, 1987; Richardson et al., 1983; Selker et al., 1990; Sheridan et al., 1989; Xie et al., 2016; Yu et al., 1996; Yu and Rosewell, 1996a; Zhang et al., 2002), monthly (Arnoldus, 1977; Ferro et al., 1991; Renard and Freimund, 1994), and annual rainfall (Bonilla and Vidal, 2011; Ferrari et al., 2005; Lee and Heo, 2011; Yu and Rosewell, 1996b). Yin et al. (2015) evaluated a number of empirical models to estimate the ~~R factor~~R-factor using rainfall data of temporal resolutions from daily to average annual, and showed that the most accurate prediction was based on data at the highest temporal resolution.

Once values of the erosivity factor is obtained with site observations, spatial interpolation methods can be used to estimate rainfall erosivity for sites without rainfall data based on surrounding sites to produce the erosivity maps or isoerodent maps. Local values of erosivity can be taken from these maps (Wischmeier and Smith, 1978). Rainfall erosivity maps can also be meaningful in various fields such as soil erosion, sediment yield, environment and ecology. ~~Erosivity maps are indispensable for regional soil erosion and erosion risk assessments based on USLE type models (Borrelli et al., 2017; Grimm et al., 2001; Liu et al., 2013; Lu et al., 2001; Panagos et al., 2015).~~ In the original version of the USLE, 181 stations with breakpoint data plus 1,700 stations with annul averaged precipitation, 1-in-2-year~~,~~ 1-h rainfall amount and 1-in-2-year~~2 yr,~~ 24-h amount ~~for eastern part of the US~~ were used to generate the erosivity map~~s~~ for the eastern part of the US (Wischmeier and Smith, 1965). In the successor of the USLE (Wischmeier and Smith, 1978), the erosivity map~~s~~ for the western part of the US were ~~added~~ generated based on 1-in-2-year~~2 yr~~, 6-h rainfall amount data (P) using the equation of $R=27.38P^{2.17}$. In Revised USLE (RUSLE), (Renard, 1997) released the erosivity map~~s~~ using the same data as Wischmeier and Smith (1965) for the eastern part, and 60-min rainfall data at 790 stations for the western part in the US. In RUSLE2, monthly erosivity maps based on 15-min data from 3,700 stations were generated (USDA-ARS, 2013). Erosvity ~~M~~maps based on spatial interpolation have been widely produced around the world (Borrelli et al., 2016; Klik et al., 2015; Liu et al., 2013; Lu and Yu, 2002; Oliveira et al., 2012; Panagos et al., 2015, 2016, 2017; Qin et al., 2016; Sadeghi et al., 2017; Yin et al., 2019~~);~~ ~~(~~Riquetti et al., 2020; Silva et al., 2020).

Recently, Food and Agriculture Organization (FAO) proposed to produce a Global Soil Erosion Map (GSERmap) which encouraged scientists from all over the world to generate their own national level maps making the most of the country knowledge, locally available methods and input data (FAO, 2019a). Rainfall erosivity maps for China were reviewed and relevant information on how they were generated are presented in Table 1, which shows that current ~~R factor~~R-factor maps for mainland China typically used readily-available daily rainfall data from about 500-800 stations (e.g., Zhang et al, 2003; Liu et al., 2013; Qin et al., 2016; Yin et al., 2019; Liu et al., 2020), which were recorded by simple rain gauges ~~and readily available~~. However, daily rainfall data are not enough to derive sub-daily intensities, which reduced the accuracy of estimated rainfall erosivity (Yin et al., 2015). ~~Breakpoint data and 1~~One-minute data are the finest resolution data measured by automatic tipping bucket rain gauges we can obtain up to now, therefore they are one of the best datasets for deriving precipitation intensity and estimating rainfall erosivity. However, 62 stations with 1-min data collected were inadequate for the spatial interpolation of rainfall erosivity over mainland China. Hourly data was believed to reflect the variation of precipitation

intensity better than daily data, which can be used to improve the estimation of at-site rainfall erosivity with precipitation observations. In addition, the increase of station density for the interpolation can better describe the spatial variation of rainfall erosivity and improve the estimation of rainfall erosivity for areas without observations together with the improvement of interpolation models and procedures.

Therefore ~~M~~more than 2,000 stations of hourly and daily data were collected, together with the 62 stations of 1-min data: (a) to develop high-precision maps of the ~~R factor~~R-factor and 1-in-10-year EI_{30} over the mainland China; (b) to quantify the improvement of the new erosivity maps in higher temporal resolution and station density and better interpolation method compared to current maps. The study of (Yin et al., 2019) was chosen to represent the latest data had set to estimate the ~~R factor~~R-factor and 1-in-10-year EI_{30} and related maps. New ~~R factor~~R-factor and 1-in-10-year EI_{30} maps were produced in this study may improve the estimation of the soil loss in mainland China. The meaning and rationale of the study is to: (1) present and share high-precision maps of the R-factor and 1-in-10-year EI_{30} over the mainland China with related earth system science communities; (2) provide some insights in the improvement of rainfall erosivity maps for other regions over the world.

Table 1~~Table 1~~: Studies on the mapping of ~~R factor~~R-factor ~~or daily rainfall erosivity(R_d)~~ for or involving China

Study Area	Period	Temporal resolution of precipitation data	No. of stations for the study area	Interpolation method	Reference
China	1956-1984	Multi-year average of annual, maximum daily and maximum hourly	125	Unknown~~Contour mapping~~	Wang et al., 1996
	1971-1998	Daily	564	Ordinary Kriging	Zhang et al., 2003
	1960-2009	Daily	590	Ordinary Kriging	Liu et al., 2013
	1951-2010	Daily	756	Universal co-kriging with the aid of the elevation	Qin et al., 2016
	1961-2016	Daily	774	Ordinary Kriging	Yin et al., 2019*
Global	1989-2010	Annual average	Gridded (0.5°×0.5°)	——	Naipal et al., 2015
	1998-2012 (in China)	Hourly and sub-hourly	3,625 (387 in China)	Gaussian Process Regression	Panagos et al., 2017
	1980-~~1999~~ ~~2000~~-2017	Daily	30,000+ (~800 in China)	Thin-plate spline smoothing	Liu et al., 2020

*Map of event 1-in-10-year EI_{30} in China was also generated.

2 Data and methods

2.1 Data

Rainfall data at three temporal resolutions were obtained hourly, daily and 1-min. Hourly data were used to generate maps of ~~R factor~~R-factor and 1-in-10-year EI_{30}. The evaluation of the effect of station density and interpolation methods on generated maps was ~~also~~ based on the erosivity calculated with hourly data. Daily rainfall data were used to adjust the erosivity estimated by hourly data when~~re~~ ~~the~~its record length was short. Data at 1-min interval were used in two ways. One was to calculate the ~~R~~

factorR-factor as true values to evaluate the effect of temporal resolution on erosivity estimation along in comparison to the hourly and the daily rainfall data. The other is to develop an exponential model for estimating R factorR-factor with the mean annual precipitation. The coefficient of the exponential model was used for adjusting the R factorR-factor values based on hourly data with of shorter periodslengths.

Rainfall data at 1-hour intervals from 2,381 meteorological stations over mainland China (Fig. 1) were collected by siphon rain gauges or tipping bucket rain gauges and quality controlled by the National Meteorological Information Center of China Meteorological Administration. The period of the data was from 1951 to 2018. The start year of the data varied because data collection commenced in different years. Observation was suspended in the snowy season, which resulted in some missing months in winter for station in the northern part of China. There were 932 (39%) stations with data for the whole year, 550 (23%) stations from April to October and 421 (18%) stations from May to September.

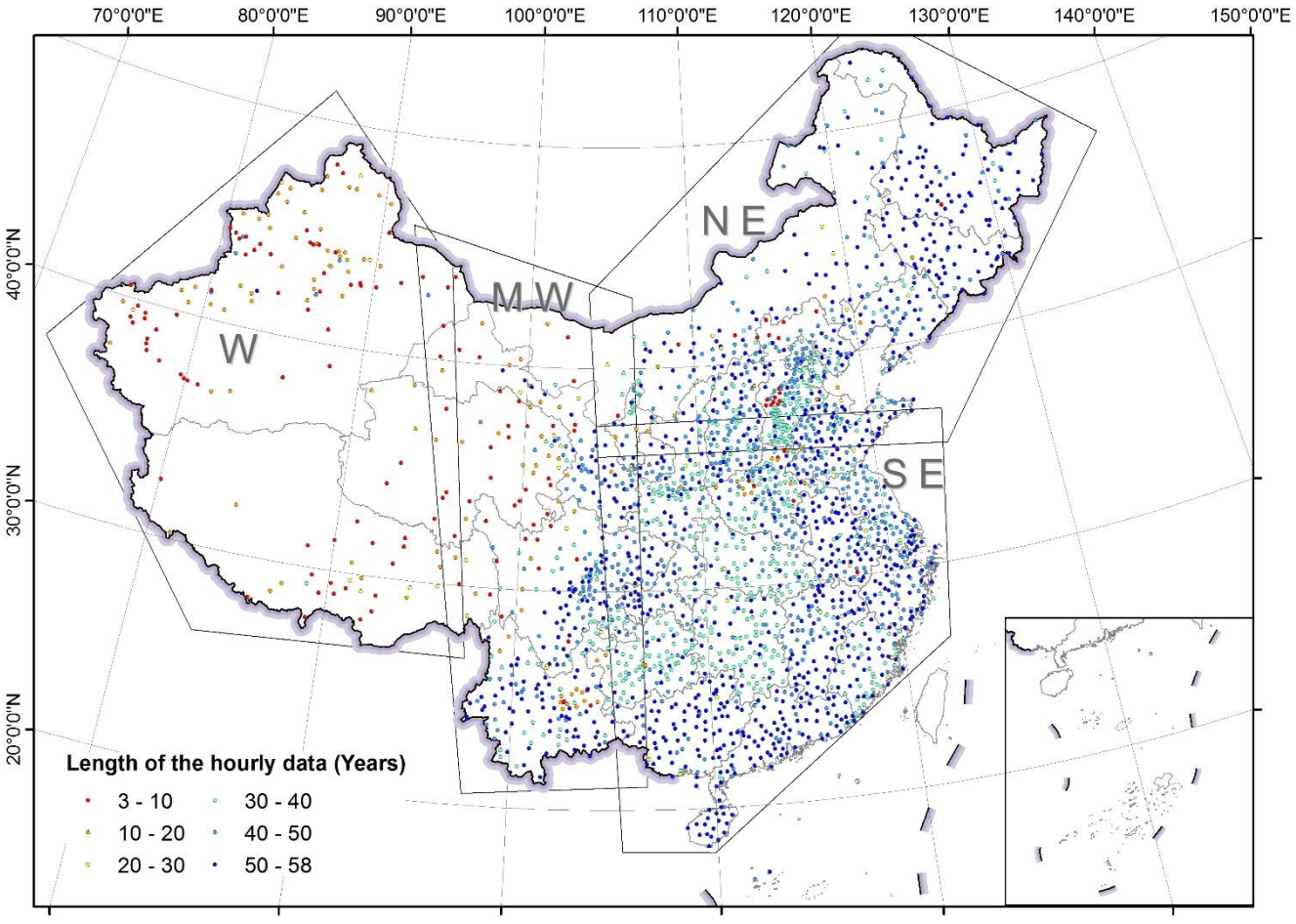

Figure 1: Spatial distribution of stations with hourly rainfall data and the length of the data. Western, Mid-western, Northeastern and Southeastern regions were abbreviated as W, MW, NE and SE, respectively.

The missing data were handled according to the following criteria: (a) a day with more than 4 missing hours was defined as a missing day; (b) a month with more than 6 missing days was defined as a missing month; (c) a year with any missing month in its wet-season was defined as a missing year. The wet-season for stations north of 32 ℃N was from May to September, and for those south of 32 ℃N was from April to October. Missing years were removed and missing hours in the remaining effective years were input in two categories: (a) the missing period is followed by a non-zero record, which recorded the accumulated rainfall amount in the missing period based on data notes; (b) the missing period is followed by zero. In the first case, each missing hour and the following non-zero hour were assigned the average value of the non-zero record in these hours. For the second case, the missing hours were input as zero value.

The daily data were obtained for the same 2,381 stations over the period of 1951-2014 (Fig. 1), and precipitation was measured with simple rain gauges. The data were also collected and quality controlled by the National Meteorological Information Center of China Meteorological Administration. Daily data were collected all year around and the number of effective years ranged from 18 to 54 years. Most of the stations (88%) have data of more than 50 years. An effective year of the daily data was defined as there is no ~~more than one~~ missing month in the year, and a missing month was defined as there are more than 6 missing days in the month. The missing records in the effective years were input as zero value.

Data at 1-min intervals were collected from 62 stations in mainland China (Fig. 2; and were used in Yue et al., 2020). Data from station No. 1-18 have effective years of 29-40 and cover the period of 1961(1971)-2000. Data from stations No. 19-62 have effective years of 2-12 and cover the period of 2005-2016. The missing data in the effective years were assumed to be zero.

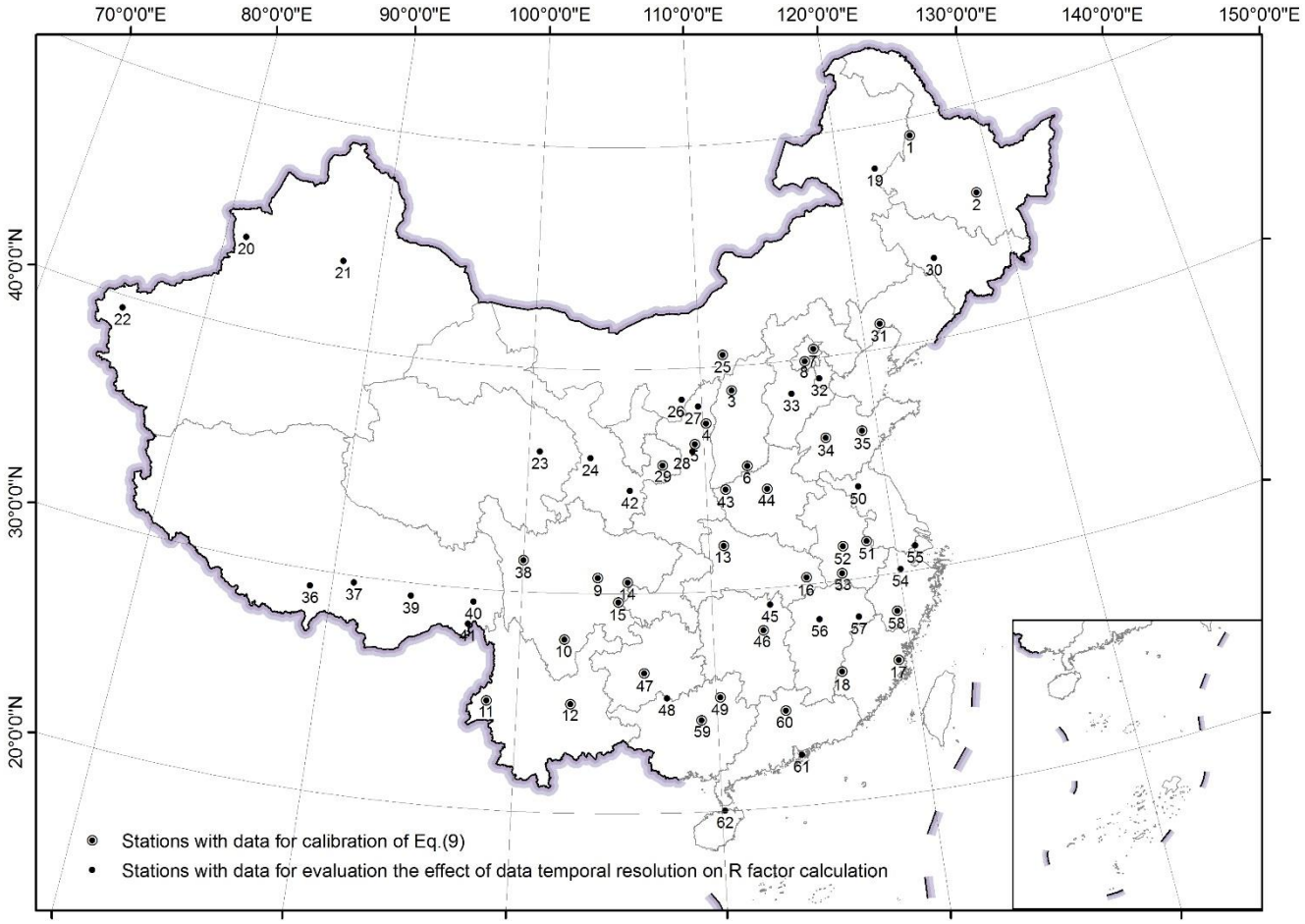

Figure 2: Spatial distribution of the stations with 1-min rainfall data

The ~~R factor~~R-factor map from Panagos et al. (2017) shown in the discussion part of this study was from the global rainfall erosivity dataset published by Joint Research Centre - European Soil Data Centre (ESDAC).

2.2 Rainfall erosivity for stations

Hourly rainfall data were first separated into rainfall storms. A continuous period of >= 6 hours of non-precipitation was regarded as the separation of two rainfall storms (Wischmeier and Smith, 1978). Storms with the amount of >= 12 mm were defined as erosive events (Xie et al., 2000), and were used to calculate the rainfall erosivity factors.

Event rainfall erosivity EI_{30} (MJ mm ha^{-1} h^{-1}) was the product of the total storm energy E (MJ ha^{-1}) and the maximum 30-min intensity I_{30} (mm h^{-1}). The maximum 1-hour intensity H_{60} (mm h^{-1}) was obtained in this study:

$$EH_{60} = E \cdot H_{60}, \quad (1)$$

$$E = \sum_{r=1}^{l}(e_r \cdot P_r), \quad (2)$$

$$e_r = 0.29[1 - 0.72exp(-0.082i_r)], \quad (3)$$

where r =1,2, …, l means that a storm could be divided into l periods or a storm lasted for l hours, e_r the unit energy (energy per mm of rainfall, MJ ha^{-1} mm^{-1}), P_r the amount (mm), and i_r the intensity (mm h^{-1}) of the r^{th} hour (USDA-ARS, 2013).

The ~~R factor~~R-factor (R_{hour}, MJ mm ha^{-1} h^{-1} a^{-1}) was the mean annual rainfall erosivity and was obtained by multiplying the ~~R factor~~R-factor from hourly data (R_h) and the conversion factor of 1.871 (Yue et al., 2020)~~:~~:

$$R_h = \frac{1}{N}\sum_{i=1}^{N}\sum_{j=1}^{m}(EH_{60})_{ij}, \quad (4)$$

$$R_{hour} = 1.871 \cdot R_h, \quad (5)$$

where i=1, 2, …, N means there are N effective years, and j = 1, 2, …, m means there are m erosive rainfall storms in the i^{th} year. ~~It was reported in Yue et al. (2020) independent 1-min rainfall data for the validation showed the symmetric mean absolute percentage error (sMAPE) was about 6.7% (ranging from 0.2% to 37.0%) after applying the conversion factor of 1.871.~~

The 1-in-10-year EI_{30} was obtained by calibrating the generalized extreme value (GEV) distribution, and the parameters of the model were estimated using L-moments method (Hosking, 1990). The GEV distribution is a family of probability distributions of Gumbel, Fréchet and Weibull. and can be denoted as G (μ, σ, ξ) with parameters μ (location), σ (scale), and ξ (shape) (Coles, 2001):

$$G(z) = exp\left\{-\left[1 + \xi\left(\frac{x-\mu}{\sigma}\right)\right]^{-1/\xi}\right\}\{x: 1 + \xi(x-\mu)/\sigma > 0\}, \quad (6)$$

where x was the annual maximum storm EI_{30} (MJ mm ha^{-1} h^{-1}), $-\infty < \mu < \infty$, $\sigma > 0$ and $-\infty < \xi < \infty$. The extreme quantiles of the annual maximum EI_{30} (X_p) were then obtained by inverting Eq. (6):

$$X_p = \begin{cases} \mu - \frac{\sigma}{\xi}\left[1 - \{-\log(1-p)\}^{-\xi}\right], for\ \xi \neq 0 \\ \mu - \sigma\log\{-\log(1-p)\}\ ,\ for\ \xi = 0 \end{cases}, \quad (7)$$

where $G(X_p) = 1 - p$. The 1-in-10-year EI_{30}, was the value of X_p when p was 1/10. The computed 1-in-10-year EI_{30} using hourly rainfall data was then multiplied by the conversion factor of 1.489 (Yue et al., 2020). ~~It was reported in Yue et al. (2020) independent 1-min rainfall data for the validation showed sMAPE was about 15.5% (ranging from 0.4% to 48.4%) after applying the conversion factor of 1.489.~~

Due to the annual ~~the~~ variability of rainfall erosivity, stations with less than 22 effective years should be excluded (Wischmeier and Smith, 1978). However, stations in western China have limited effective years, with 133 out of 150 stations having less than 22 effective years (Fig. 1). Once stations with less than 22 effective years are removed, the western stations would be too sparse, which would reduce the interpolation accuracy of the rainfall erosivity map. To fill the gap of the insufficient years, daily rainfall data observed by simple rainfall gauges (usually have longer periods) of ~~these~~the same stations were used.

The calculation of the ~~R factor~~R-factor considered the following two cases: (1) The effective years of hourly data were no less than those of daily data (871 out ~~37%~~ of 2,381~~the~~ stations); (2) The effective years of hourly data were less than those of daily data (1,510 out~~63%~~ of ~~the~~ 2,381 stations). In the first case, the ~~R factor~~R-factor was calculated directly by hourly data with Eq. (1-5). In the second case, the ~~R factor~~R-factor was firstly calculated by hourly data with Eq. (1-5), then adjusted by the mean annual rainfall calculated by hourly and daily data following (Zhu and Yu, 2015):

$$R_{\mathrm{h\_adj}} = R_{hour}\left(\frac{P_d}{P_h}\right)^{1.481}, \quad (8)$$

where R_{h_adj} was the adjusted ~~R-factor~~R-factor, R_{hour} was the estimated ~~R-factor~~R-factor using hourly rainfall data with Eq. (1-5), P_d was the mean annual precipitation of longer period (period of the daily data), and P_h was the mean annual precipitation of shorter period (period of the hourly data).

The exponent value of 1.481 was estimated~~calibrated~~ based on a power relationship between the mean annual precipitation and~~with~~ the R-factor, and the latter was determined using 1-min and daily rainfall data of 35 stations in China (Fig. 2). All the daily and 1-min data shared ~~a power function (Eq. 9; R^2 = 0.776) of the mean annual precipitation and R-factor~~rainfall erosivity ~~using 1-min and daily rainfall data of 35 stations in China (Fig. 2), which had~~. ~~The 1-min and daily data share~~ common periods of record of more than 10 years ~~for these 35 stations~~.

$$R_{min} = 0.156 \cdot P_m^{1.481}, \quad (9)$$

where R_{min} was the ~~R-factor~~R-factor (MJ mm ha^{-1} h^{-1} a^{-1}), and P_m was the mean annual precipitation (mm) using 1-min data. The coefficient of determination (R^2) was 0.776 for Eq. 9. ~~An analysis based on a random sample process following (??) showed the adjusting process on R-factor for stations with short lengths of hourly data decreased the absolute relative error of about 0~20%, depending on the annual variability of rainfall erosivity.~~ ~~The model was tested by daily rainfall data over China to improve the accuracy of the R-factor by 0-20%.~~

~~R-factor~~R-factor based on 1-min rainfall data was calculated using Eq. (10-11):

$$R_{min} = \frac{1}{N}\sum_{i=1}^{N}\sum_{j=1}^{m}(EI_{30})_{ij}, \quad (10)$$

$$\mathrm{E}I_{30} = E \cdot I_{30}, \quad (11)$$

where I_{30} was the maximum continuous 30-min intensity. Total storm energy (E) was obtained ~~also~~ using methods from RUSLE2 as Eq. (2-3) with a time increment of 1 min.

Calculation of the 1-in-10-year EI_{30} also considered two cases: (1) The effective years of the hourly data were no less than 22 years (89% of the stations) and the 1-in-10-year EI_{30} was estimated by hourly data with Eqs. (6-7); (2) The effective years of the hourly data were less than 22 years, but those of the daily data were no less than 22 years (11%), the 1-in-10-year EI_{30} was estimated by daily data as follows. Firstly, daily rainfall erosivity was obtained by the following equation developed by Xie et al. (2016):

$$R_{daily} = \alpha P_{daily}^{1.7265}, \quad (12)$$

where P_{daily} was the daily precipitation (≥10mm), parameter α was 0.3937 in the warm season (May to September), and 0.3101 in the cold season (October to April). Secondly, the 1-in-10-year daily erosivity was obtained by calibrating the GEV distribution parameters as Eq. (6-7) and the *x* in the functions was replaced by the annual maximum daily erosivity. Finally, the 1-in-10-year daily erosivity from daily data was multiplied by a conversion factor of 1.17 to correct the 1-in-10-year daily erosivity to approximate the actual event 1-in-10-year EI_{30} from 1-min data (Yin et al., 2019). The record length was 22 to 29

for 16 (0.7%) stations, 30 to 39 for 44 (1.8%) stations, 40 to 49 for 216 stations (9.1%) stations, more than 50 for 2,105 (88.4%) stations when these adjustments were made.

2.3 Spatial interpolation and cross validation

Since there is a good correlation between erosivity factor and the mean annual precipitation, the erosivity maps were obtained using the method of Universal Kriging with the annual rainfall as a co-variable. The annual average rainfall was computed using daily rainfall data of the stations and was firstly interpolated using Ordinary Kriging, and the results were used to conduct Universal Kriging. Both the mean annual precipitation and the erosivity factors were interpolated first for each region separately (Fig. 1; Li et al., 2014), and then combined to obtain annual precipitation and erosivity maps over China. Buffer areas were used to avoid the discontinuity in the boundary areas following Li et al. (2014).

To evaluate the efficiency of interpolation models, a leave-one-out cross-validation method was applied in each region. Symmetric mean absolute percentage error (sMAPE) and Nash-Sutcliffe model efficiency coefficient (NSE) were used for the assessment:

$$\text{sMAPE} = \frac{1}{n}\sum_{i=1}^{n}\left|\frac{F_i - A_i}{(F_i + A_i)/2}\right| \times 100\%, \quad (13)$$

$$\text{NSE} = 1 - \frac{\sum_{i=1}^{n}(F_i - A_i)^2}{\sum_{i=1}^{n}(A_i - \overline{A_i})^2}, \quad (14)$$

where n was the number of stations, F_i was the predicted value at the position of the i[th] station using data from surrounding stations, A_i was the observed~~true~~ value at the i[th] station.

2.4 The evaluation of the improvement on the accuracy of the erosivity maps

Current erosivity mapping at the national scale in mainland China usually uses daily rainfall data from about 500-800 stations.~~more than 700 stations.~~ The ~~R factor~~R-factor and 1-in-10-year EI_{30} maps of Yin et al. (2019) were taken as references to evaluate the improvement in the accuracy of the erosivity maps generated in this study. To compare the accuracy of the erosivity maps of this study and those of Yin et al. (2019), true R-factor values using~~from~~ 1-min data and~~using~~ Eq. (10-11) for 62 stations were used to evaluate the improvement of ~~R factor~~R-factor. For 1-in-10-year EI_{30}, ~~and those from~~ 1-min data for 18 stations (No.1-18; Fig. 2~~Figure 2~~) with more than 22 years were used ~~to evaluate the 1-in-10-year EI_{30}~~. The cross-validation values ~~extracted~~ from the interpolation of~~from~~ the two erosivity maps ~~for these stations~~ were compared with the true values calculated with 1-min data to calculate relative error for these stations. ~~Relative error (%) for each station was calculated as follows:~~

~~$$RE_{ij} = \frac{R_{ij} - (R_{min})_i}{(R_{min})_i} \times 100\%, \quad (15)$$~~

~~where $(R_{min})_i$ is the true value calculated from 1-min data, $i = 1,2, \ldots, 62$ (18); R_{ij} was the value extracted from the erosivity map of this study and that of ; $j = 1,2,3,4$ represents R-factor and 1-in-10-year EI_{30} maps for the two studies; RE_{ij} was the relative error (%) of the R-factor or 1-in-10-year EI_{30} of the i_{th} station on the j_{th} map~~. Considering that the absolute values of

relative errorRE would be high for stations with smaller R factorR-factor values, the relative error of the entire map was expressed as the median absolute value of the relative errorRE for all the stations.

The erosivity maps in this study used a different procedure as in Yin et al. (2019) mainly in three areas: (1) temporal resolution (hourly vs. daily); (2) number of stations (2,381 stations vs. 744 stations); (3) interpolation method (Universal Kriging vs. Ordinary Kriging).

To evaluate the effect of the temporal resolution on the calculated R factorR-factor and 1-in-10-year EI_{30}, hourly and daily rainfall data with the same period as the 1-min data at the 62 stations were used. R factorR-factors from hourly data were based on Eq. (1-5), those from daily rainfall data were based on Eq. (12), and those from 1-min data were based on Eq. (10-11). The 1-in-10-year EI_{30} were all calculated by calibrating GEV distribution using Eq. (6-7). Erosivity factors from 1-min data can be regarded as the true values. The relative error was computed for evaluating accuracy.

To evaluate the effect of station density, hourly data from 774 stations (used in Yin et al. (2019)) and from 2,381 stations (used in this study) were used to generate two separate erosivity maps. R factorR-factor and 1-in-10-year EI_{30} values were compared using leave-one-out cross validation method region by region. The sMAPE was calculated for accuracy assessment.

To evaluate the effect of interpolation methods, Ordinary Kriging and Universal Kriging with the mean annual rainfall as the co-variable was were applied for the R factorR-factor and 1-in-10-year EI_{30} computed using hourly data from 2,381 stations. Both interpolation methods were applied to each of four different regions as shown in Fig. 1 and leave-one-out cross validation results were compared. The sMAPE was also calculated to evaluate the accuracy of interpolated values.

The framework of this study is shown in Fig. 3.

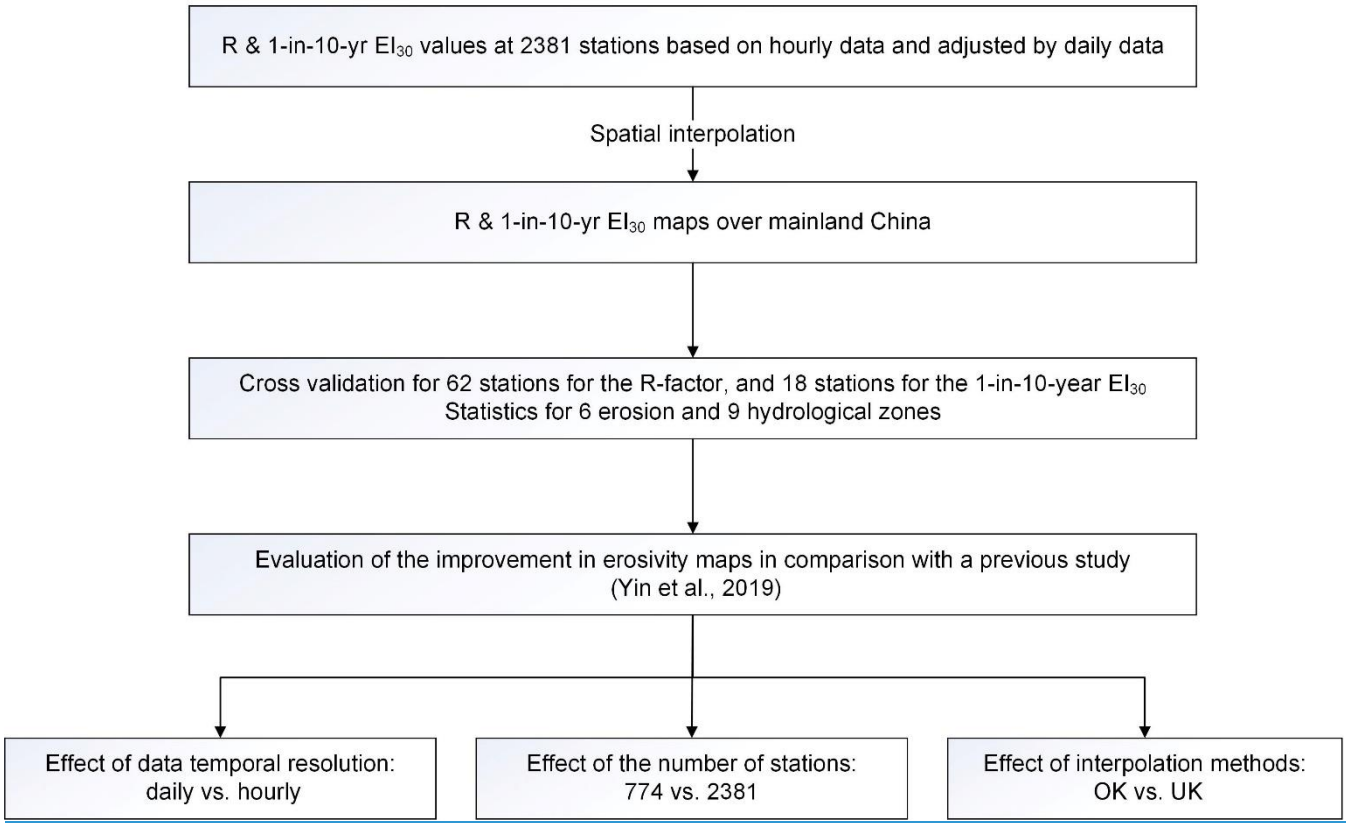

Figure 3: Framework of this study

3 Results

3.1 Accuracy evaluation on erosivity maps

Taking erosivity maps (~~R factor~~R-factor and 1-in-10-year EI_{30}) generated by Yin et al. (2019) as references, this study shows a certain improvement in accuracy (Fig. 4~~3~~; Table 2~~ Table 2~~). For the ~~R factor~~R-factor, the values in the map of Yin et al. (2019) were underestimated where the ~~R factor~~R-factor was relatively high, and overestimated where the ~~R factor~~R-factor was relatively low. The improvement was particularly noticeable for western China ($R < 1{,}000$ MJ mm ha^{-1} h^{-1} a^{-1}) and the southeastern coastal region ($R > 10{,}000$ MJ mm ha^{-1} h^{-1} a^{-1}).

Relative errors of the two maps at the 62 stations are shown in Fig. ~~4~~ 5 (a) and (b). Those with the relative error of more than 100% were all in the ~~western~~ Western (W) or Mid-western (MW) region. There was no obvious~~The~~ difference between the median values (also the average values) of the absolute relative error ~~RE in Mid-western (MW), Northeastern (NE) and Southeastern (SE) regions were 15.9% and 19.4%~~ for the R-factor~~maps~~ in this study and Yin et al. (2019) in Mid-western

(MW), Northeastern (NE) and Southeastern (SE) regions (Table 2), however, there are some ex~~r~~tremely high relative error values in Yin's map which were found to be located in the MW region (Fig. 5(a)). ~~indicating an improvement of 3.4%.~~ The median values of the absolute relative error ~~ose~~ in Western (W) region were 16.2~~21.6~~% and 161.6~~45.2~~%, respectively for this study and Yin et al. (2019), which~~and~~ indicat~~ed~~~~ing~~ an improvement of 145.4~~23.6~~%. For 1-in-10-year EI_{30}, the median values of the absolute relative error~~RE~~ were 13.5~~0~~% for ~~maps from~~ this study and 20.6~~21.7~~% for Yin et al. (2019), indicating an improvement of 7.1~~8.7~~% in the mid-western and eastern regions (Table 2, (Fig. 5(b)). The relative errors of the 1-in-10-year EI_{30} in this study concentrated in the range of -1~~2~~0% ~ +1~~2~~0%, whereas those in Yin et al. (2019) concentrated ~~have a higher frequncy at~~ in the range of ~~±~~ -25% ~ ~~2~~-15~~0~~% ~~,~~and -+15% ~ +25%~~instead of 0~~ (Fig. 5(c)). The evaluation on the 1-in-10-year EI_{30} map didn't cover the western region where there were no 1-min data with enough effective years to estimate the return level. The spatial distribution of the absolute relative errors of the maps from this study is shown in Fig. 6.

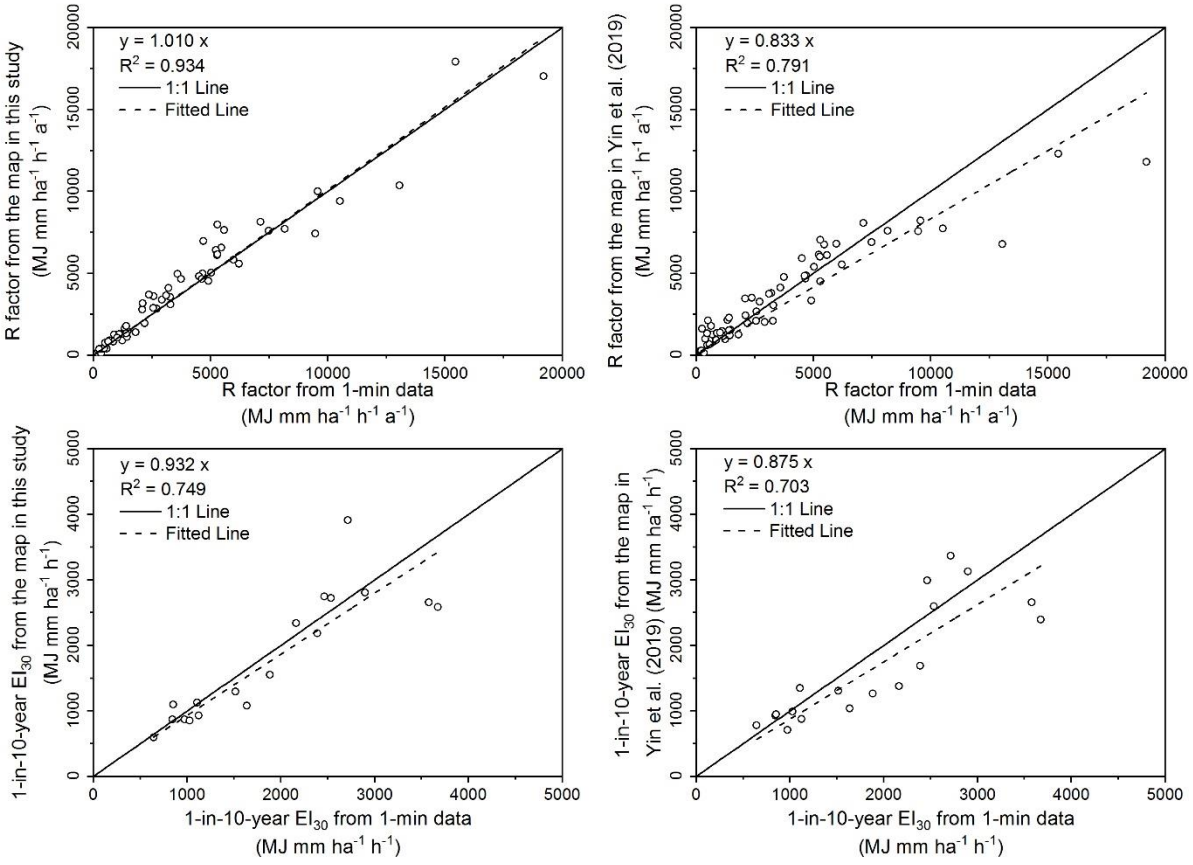
y = 1.010 x
R² = 0.934
1:1 Line
Fitted Line
R factor from the map in this study (MJ mm ha⁻¹ h⁻¹ a⁻¹)
R factor from 1-min data (MJ mm ha⁻¹ h⁻¹ a⁻¹)
y = 0.833 x
R² = 0.791
1:1 Line
Fitted Line
R factor from the map in Yin et al. (2019) (MJ mm ha⁻¹ h⁻¹ a⁻¹)
R factor from 1-min data (MJ mm ha⁻¹ h⁻¹ a⁻¹)
y = 0.932 x
R² = 0.749
1:1 Line
Fitted Line
1-in-10-year EI30 from the map in this study (MJ mm ha⁻¹ h⁻¹)
1-in-10-year EI30 from 1-min data (MJ mm ha⁻¹ h⁻¹)
y = 0.875 x
R² = 0.703
1:1 Line
Fitted Line
1-in-10-year EI30 from the map in Yin et al. (2019) (MJ mm ha⁻¹ h⁻¹)
1-in-10-year EI30 from 1-min data (MJ mm ha⁻¹ h⁻¹)

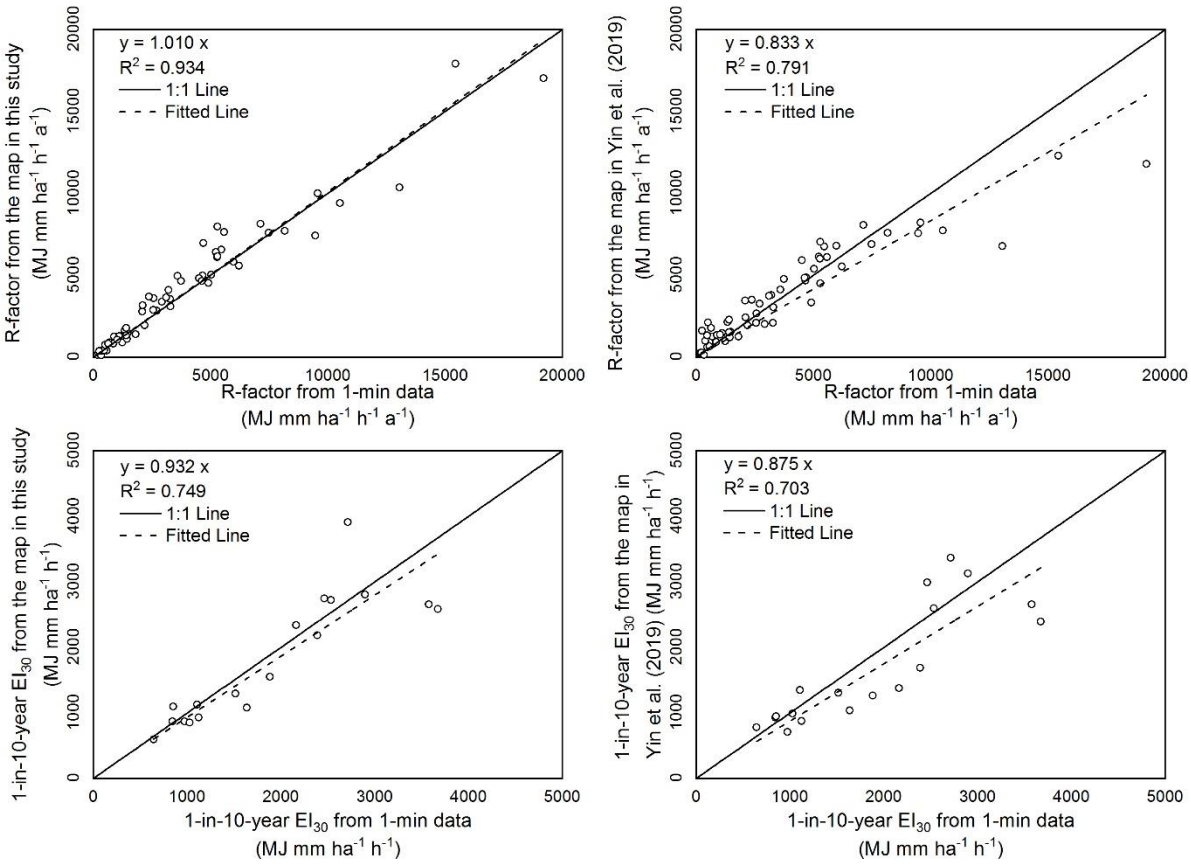

Figure 4: Comparison of the ~~R-factor~~R-factors and 1-in-10-year EI_{30} extracted from the maps and the true values. The graphs on the left were the evaluation of the maps generated in this study, and those on the right were the evaluation of the maps generated by Yin et al. (2019)

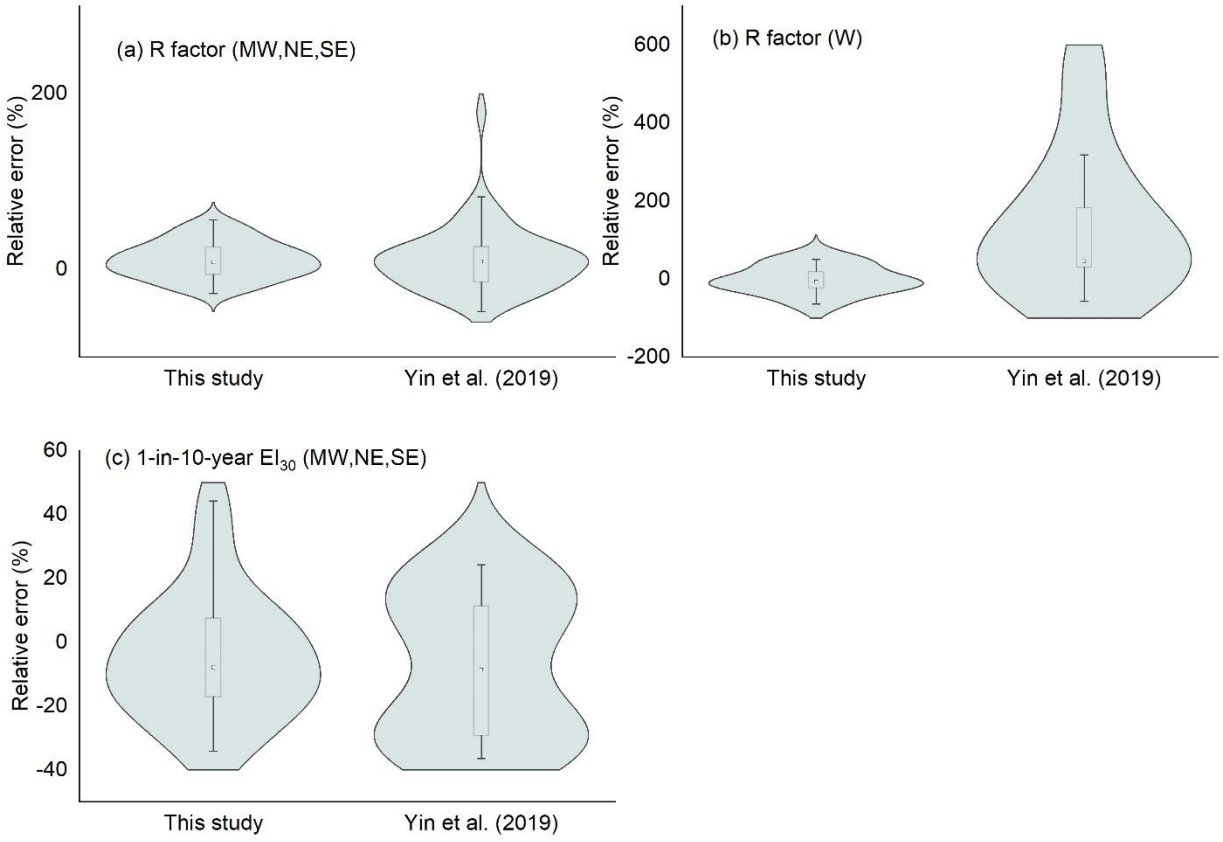
(a) R factor (MW,NE,SE)
Relative error (%)
200
0
This study
Yin et al. (2019)
(b) R factor (W)
Relative error (%)
600
400
200
0
-200
This study
Yin et al. (2019)
(c) 1-in-10-year EI_{30} (MW,NE,SE)
Relative error (%)
60
40
20
0
-20
-40
This study
Yin et al. (2019)

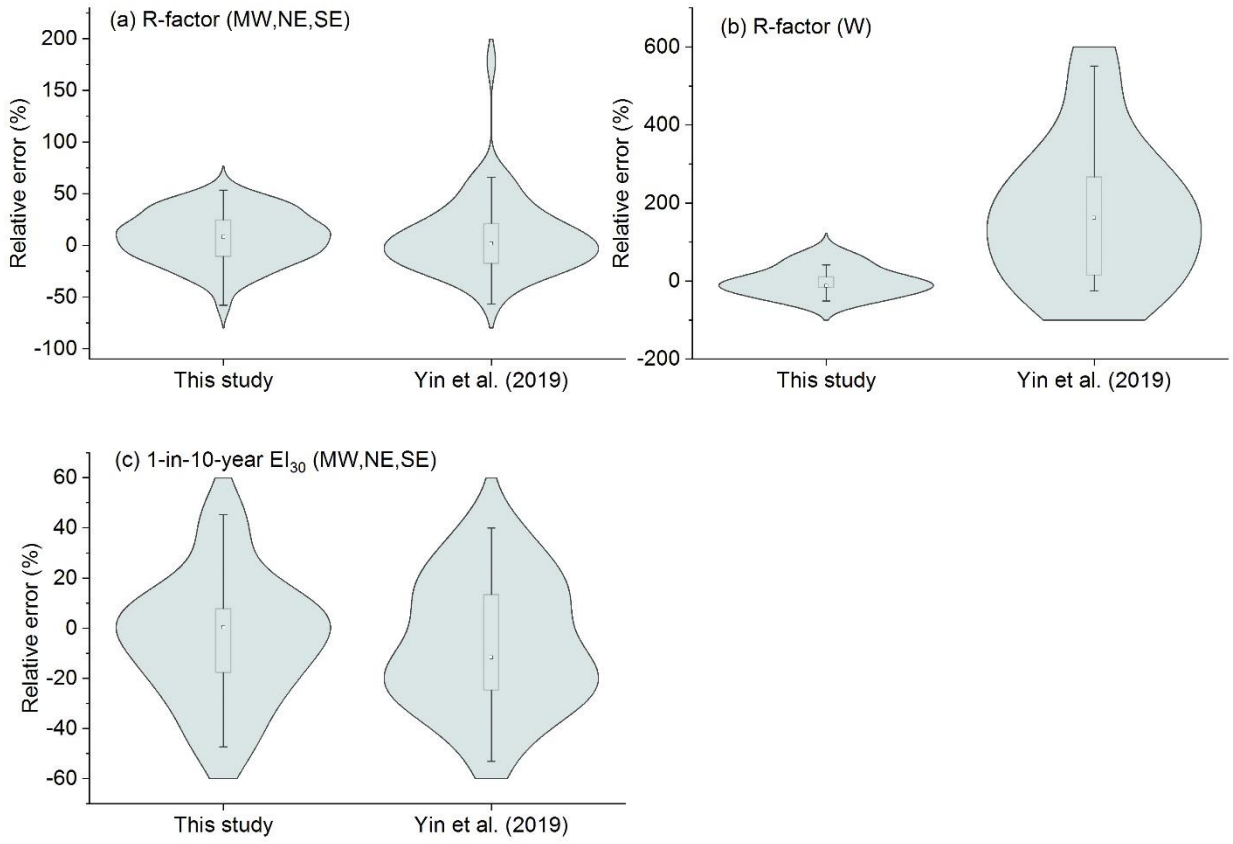

Figure 5: The relative errors of the ~~R factor~~R-factor~~s~~ (a for region MW, NE, SE; b for region W) and 1-in-10-year EI_{30} (c for region ME, NE, SE) ~~extracted from the~~ maps

Table 2: The statistical characteristics of the absolute relative errors of the erosivity factors from the maps

	~~R factor~~R-factor				1-in-10-year EI_{30}	
	MW, NE, SE		W		MW, NE, SE	
	This study	Yin et al. (2019)	This study	Yin et al. (2019)	This study	Yin et al. (2019)
25th percentile	9.3%~~6.2%~~	8.8%~~10.5%~~	11.4%~~9.3%~~	23.1%~~29.9%~~	5.1%~~7.5%~~	13.0%~~11.1%~~
Median	17.8%~~15.9%~~	18.1%~~19.4%~~	16.2%~~21.6%~~	161.6%~~45.2%~~	13.5%~~13.0%~~	20.6%~~21.7%~~
75th percentile	32.8%~~27.8%~~	34.4%~~32.8%~~	45.9%~~39.1%~~	292.3%~~250.2%~~	31.6%~~26.6%~~	31.3%~~30.2%~~
Mean	21.0%~~19.5%~~	24.7%~~27.2%~~	28.7%~~23.4%~~	184.8%~~150.6%~~	18.6%~~16.2%~~	22.3%~~21.2%~~

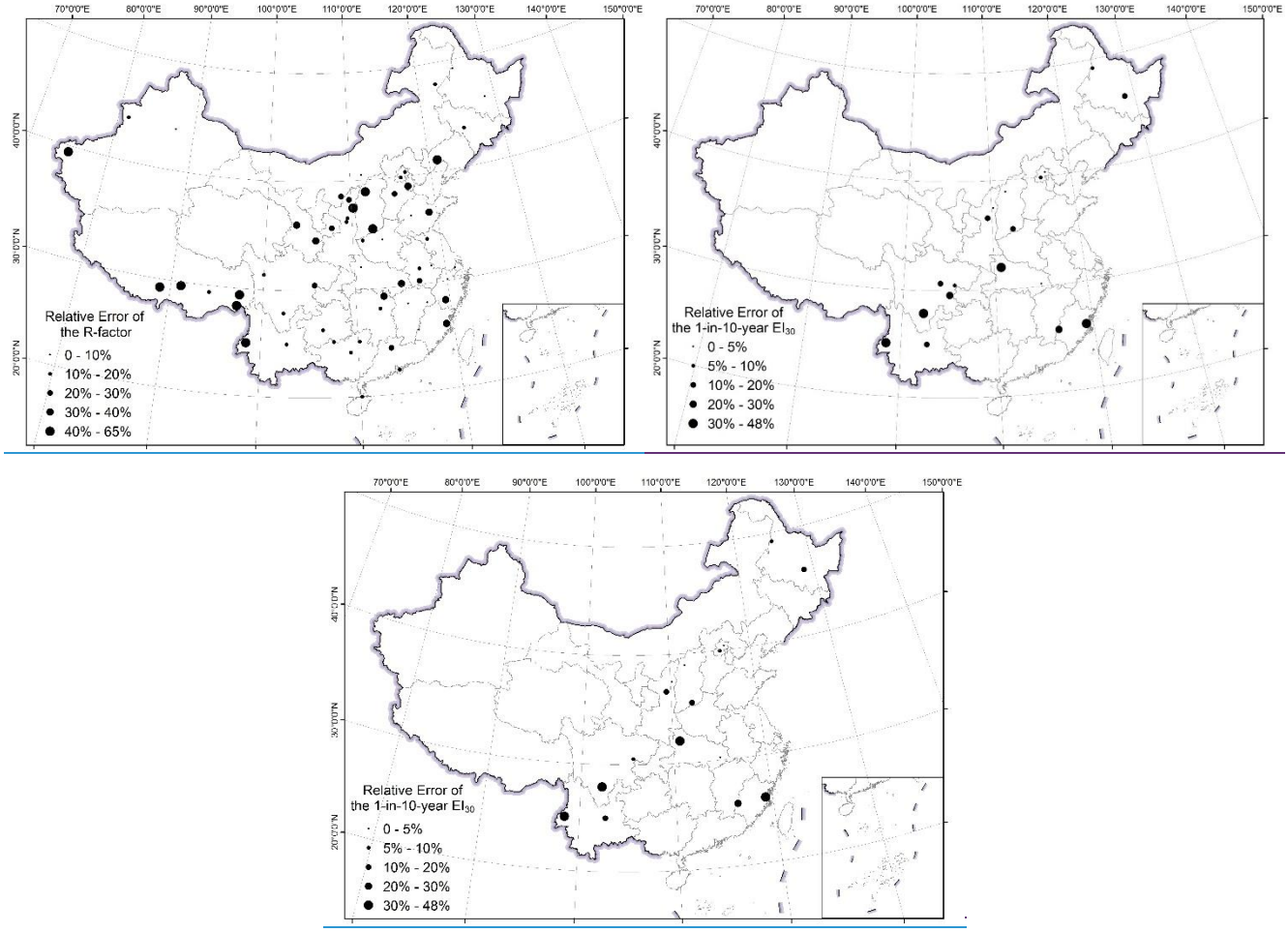

(a) R-factor (b) 1-in-10-year EI_{30}

Figure 6: Spatial distribution of the absolute relative errors in the map of R-factor ~~from~~ for 62 stations ~~for R-factor~~ (a) and in the map of ~~18 stations for~~ 1-in-10-year EI_{30} for 18 stations (b) with 1-min observation data.

3.2 Erosivity maps and the differences~~changes~~ comparing with the previous study

The ~~R-factor~~R-factor generally decreased from the southeastern part to the northwestern part of China (Fig. ~~5a~~7a), ranging from 0 to 25,300 MJ mm ha^{-1} h^{-1} a^{-1}. The map of 1-in-10-year EI_{30} shows a similar spatial pattern with that of the ~~R-factor~~R-factor (Fig. ~~5b~~7b), ranging from 0 to 11,246 MJ mm ha^{-1} h^{-1}. Zero ~~R-factor~~R-factor value is found at Turpan, Xinjiang Province, where the mean annual rainfall is only 7.8 mm. The maximum of the ~~R-factor~~R-factor (more than 20,000 MJ mm ha^{-1} h^{-1} a^{-1}) is located in the southern part of the Guangxi and Guangdong provinces, along the South China Sea, where the mean annual rainfall is more than 2,500 mm.

In addition to the overall trend, some local scale characteristics could be identified in the maps. Taking the ~~R factor~~R-factor map as an example, in the western region, the wetter region in northwestern China was located in the west of Dzungaria Basin and along the Tianshan Mountain, which could be captured on the map. Some statistical characteristics of the new maps of the erosivity factors are shown in Table 3 based on soil erosion and hydrological zoning schemes (Fig. 8).

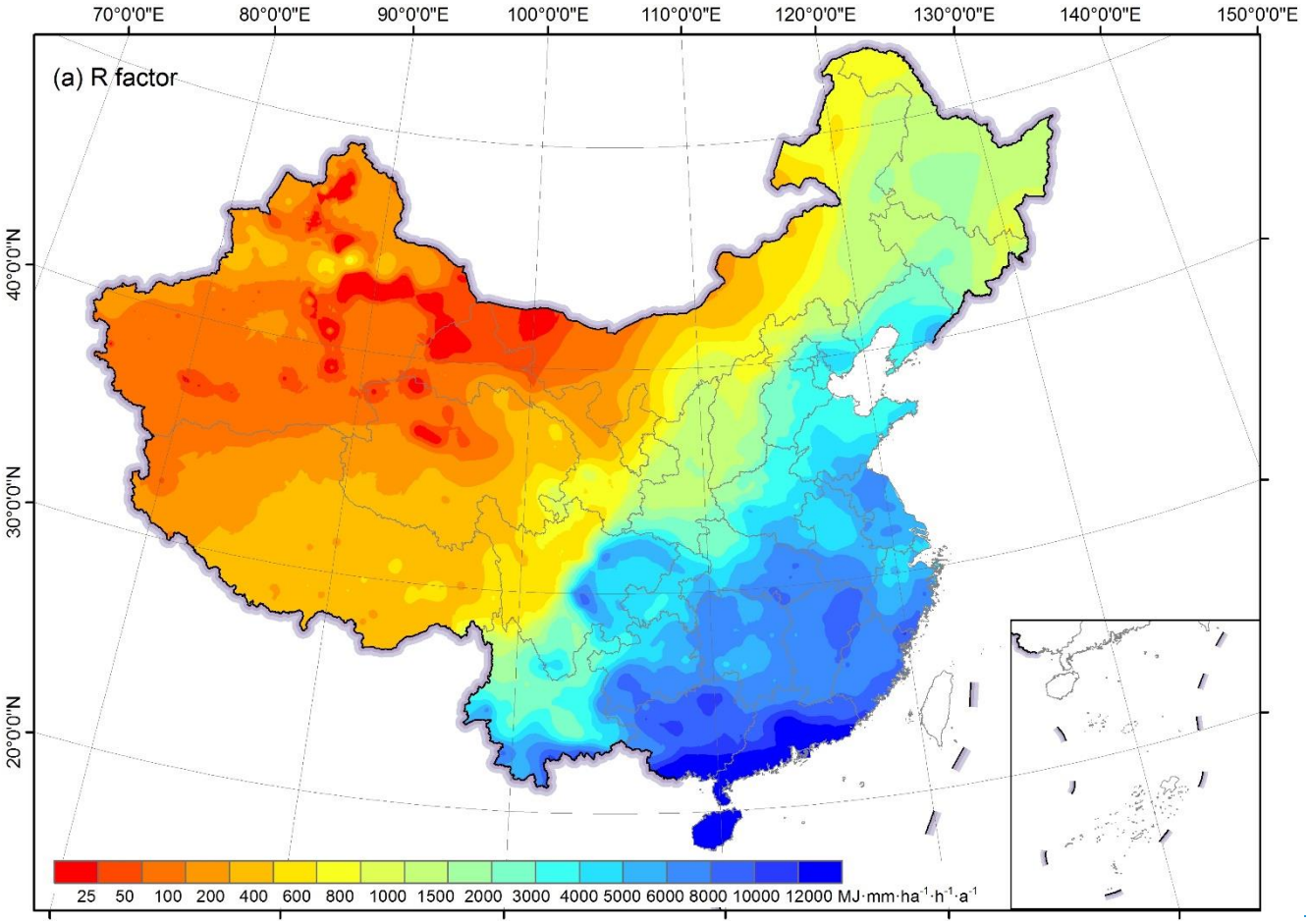
(a) R factor
70°0'0"E
80°0'0"E
90°0'0"E
100°0'0"E
110°0'0"E
120°0'0"E
130°0'0"E
140°0'0"E
150°0'0"E
40°0'0"N
30°0'0"N
20°0'0"N
25 50 100 200 400 600 800 1000 1500 2000 3000 4000 5000 6000 8000 10000 12000 MJ·mm·ha-1·h-1·a-1

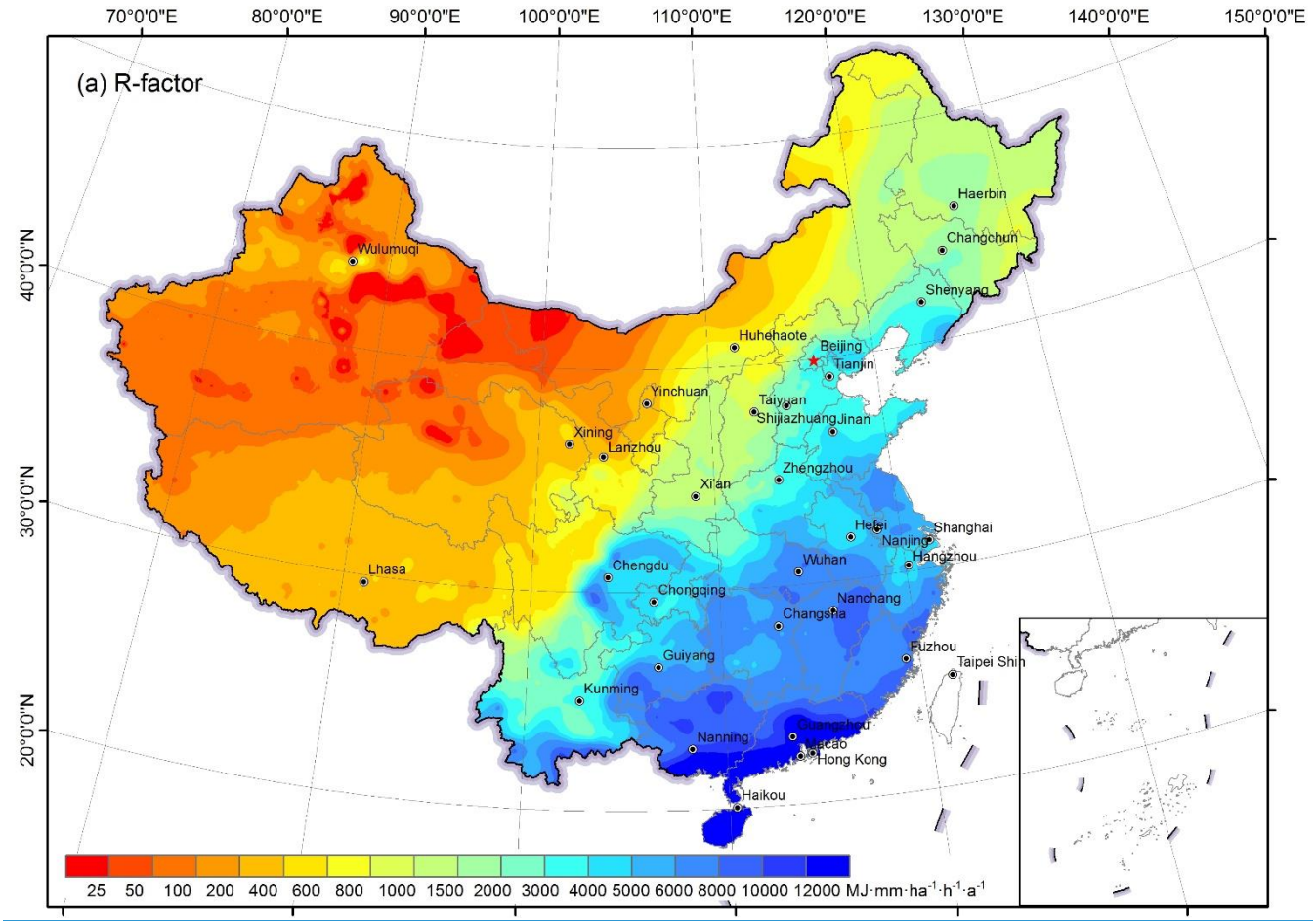
(a) R-factor
70°0'0"E
80°0'0"E
90°0'0"E
100°0'0"E
110°0'0"E
120°0'0"E
130°0'0"E
140°0'0"E
150°0'0"E
40°0'0"N
30°0'0"N
20°0'0"N
Wulumuqi
Haerbin
Changchun
Shenyang
Huhehaote
Beijing
Tianjin
Yinchuan
Taiyuan
Shijiazhuang
Jinan
Xining
Lanzhou
Zhengzhou
Xi'an
Hefei
Shanghai
Nanjing
Hangzhou
Lhasa
Chengdu
Wuhan
Chongqing
Nanchang
Changsha
Fuzhou
Taipei Shih
Guiyang
Kunming
Guangzhou
Macao
Hong Kong
Nanning
Haikou
25 50 100 200 400 600 800 1000 1500 2000 3000 4000 5000 6000 8000 10000 12000 MJ·mm·ha-1·h-1·a-1

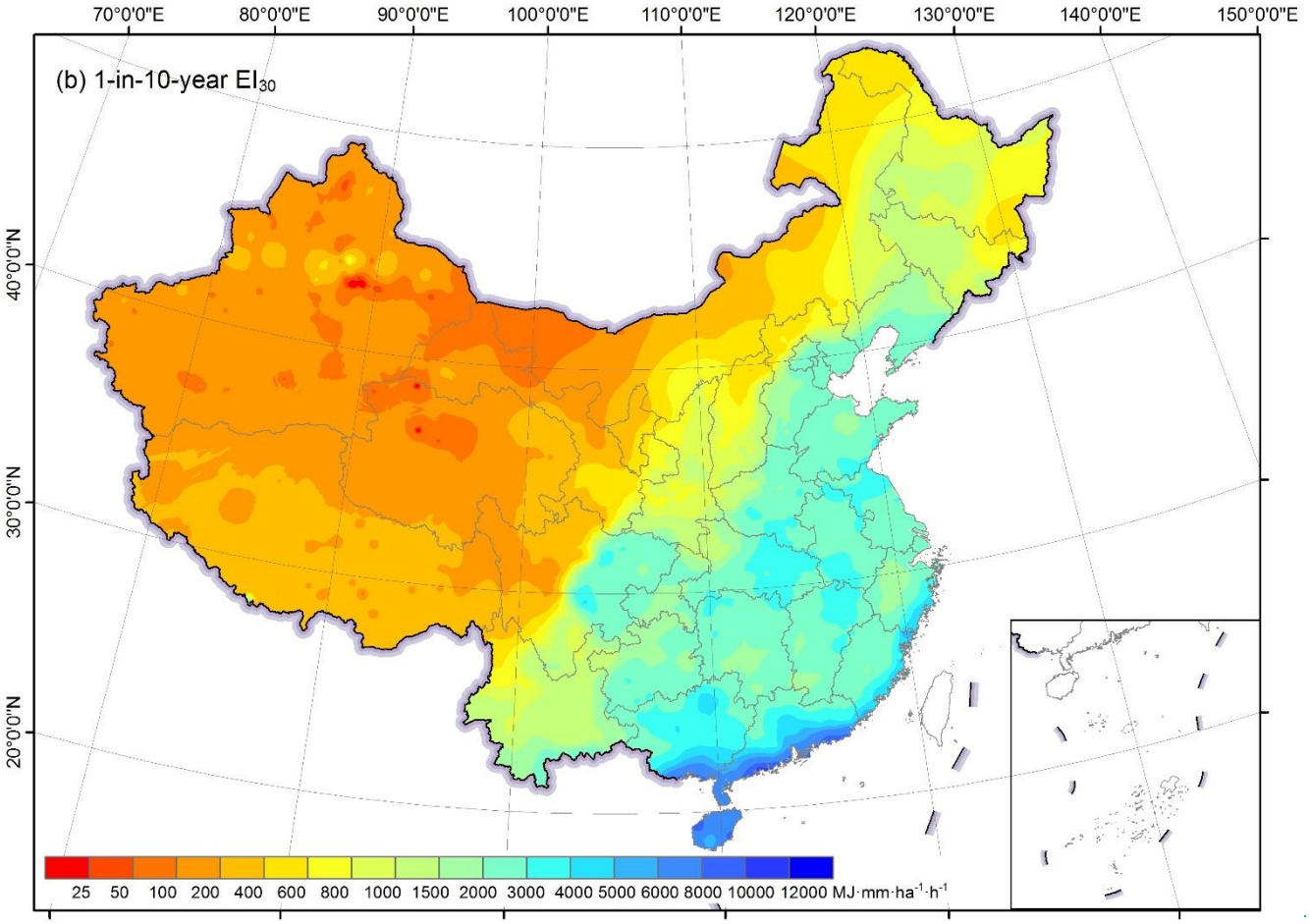
(b) 1-in-10-year EI_{30}
70°0'0"E
80°0'0"E
90°0'0"E
100°0'0"E
110°0'0"E
120°0'0"E
130°0'0"E
140°0'0"E
150°0'0"E
40°0'0"N
30°0'0"N
20°0'0"N
25 50 100 200 400 600 800 1000 1500 2000 3000 4000 5000 6000 8000 10000 12000 MJ·mm·ha^{-1}·h^{-1}

330

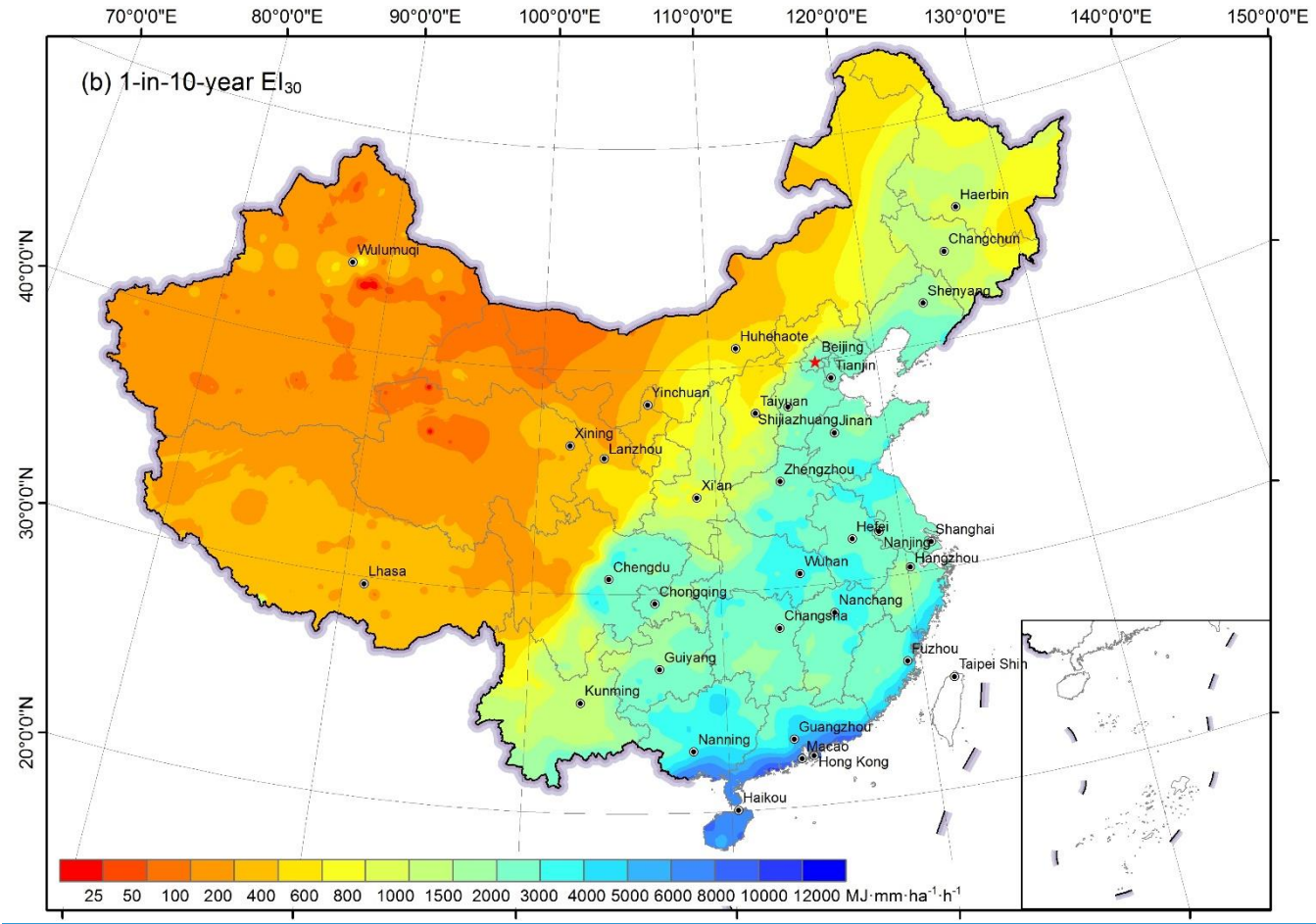

Figure 7: ~~R factor~~R-factor(a) and 1-in-10-year EI_{30}(b) over mainland China based on hourly data from 2381 stations

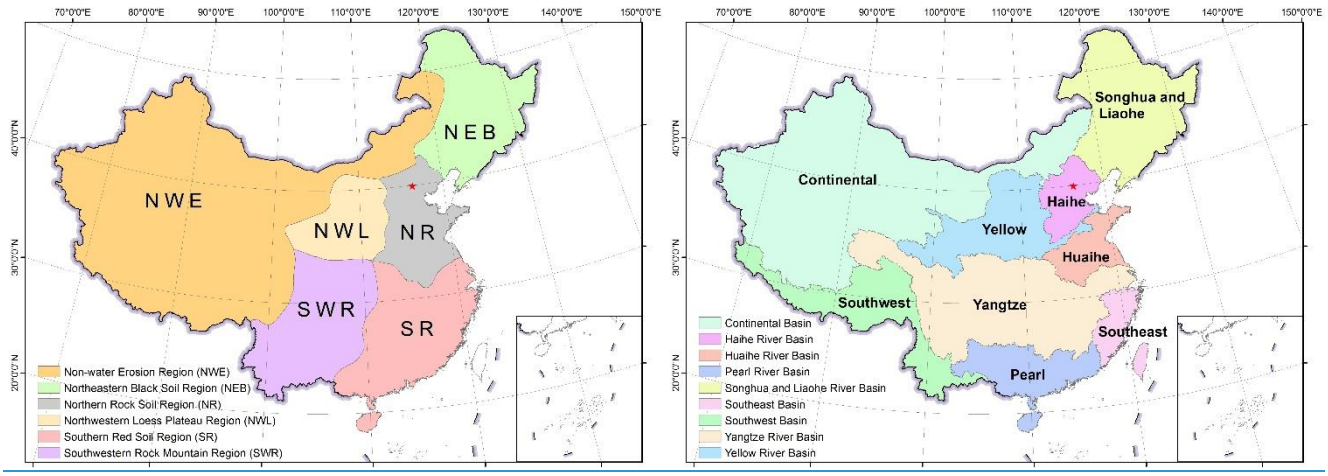

(a) Soil erosion zoning **(b) Hydrological zoning**

335 **Figure 8: Zoning schemes**

Table 3: Statistical characteristics of R-factor and 1-in-10-year EI_{30} in soil erosion and hydrological zonings

Factors	Zones	Mean	Std.	5th-percentile	25th-percentile	50th-percentile	75th-percentile	95th-percentile
R-factor	Mainland China	2200	3147	47	147	645	3503	8208
(MJ mm ha^{-1} h^{-1} a^{-1})	NWE	208	192	30	70	144	276	614
	NWL	896	431	263	549	875	1239	1562
	NR	3637	1443	935	2780	3747	4577	5946
	NEB	1483	766	671	1041	1311	1611	3284
	SWR	4226	2079	841	2610	4324	5503	8060
	SR	8294	3370	4918	6140	7311	9141	16544
	Continental	138	130	25	62	92	174	424
	Haihe	2437	1169	719	1218	2717	3489	4042
	Huaihe	4744	948	3197	4062	4653	5466	6310
	SongLiao	1405	765	623	952	1235	1553	3220
	Yellow	920	754	214	402	749	1205	2199
	Yangtze	3933	2535	215	1355	4508	6052	7666
	Southwest	1318	2043	132	265	316	940	5998
	Southeast	7069	1292	4964	6014	7192	7916	9110
	Pearl	10280	3967	4450	7697	9354	12731	17591
1-in-10-year EI_{30}	Mainland China	1040	1259	99	166	435	1766	3206
(MJ mm ha^{-1} h^{-1})	NWE	189	101	84	125	165	220	415
	NWL	635	254	226	438	635	825	1031
	NR	2199	770	556	1860	2422	2717	3123
	NEB	948	449	444	669	867	1044	2055
	SWR	1706	766	439	1098	1689	2308	2952
	SR	3273	1418	1953	2375	2846	3512	6814
	Continental	164	84	80	114	140	193	363
	Haihe	1595	794	459	718	1773	2350	2626
	Huaihe	2706	394	1999	2465	2723	2957	3337
	SongLiao	902	453	422	604	823	1026	1974
	Yellow	627	472	182	293	525	813	1430
	Yangtze	1706	1039	167	711	1959	2551	3194
	Southwest	496	533	184	212	232	389	1701
	Southeast	2814	881	1781	2160	2550	3262	4570
	Pearl	3846	1822	1564	2604	3320	4698	7512

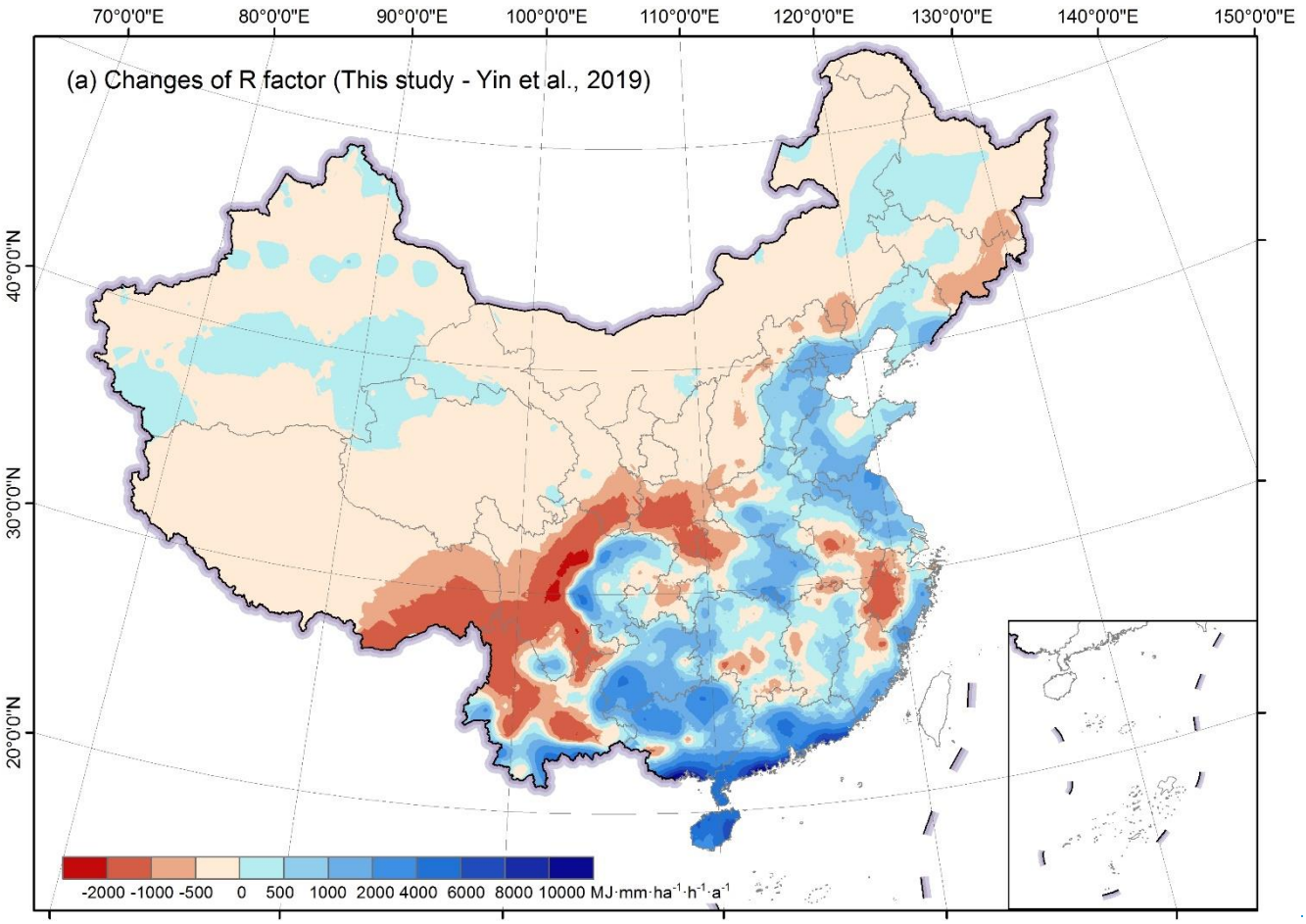
(a) Changes of R factor (This study - Yin et al., 2019)
70°0'0"E
80°0'0"E
90°0'0"E
100°0'0"E
110°0'0"E
120°0'0"E
130°0'0"E
140°0'0"E
150°0'0"E
40°0'0"N
30°0'0"N
20°0'0"N
-2000 -1000 -500 0 500 1000 2000 4000 6000 8000 10000 MJ·mm·ha-1·h-1·a-1

340

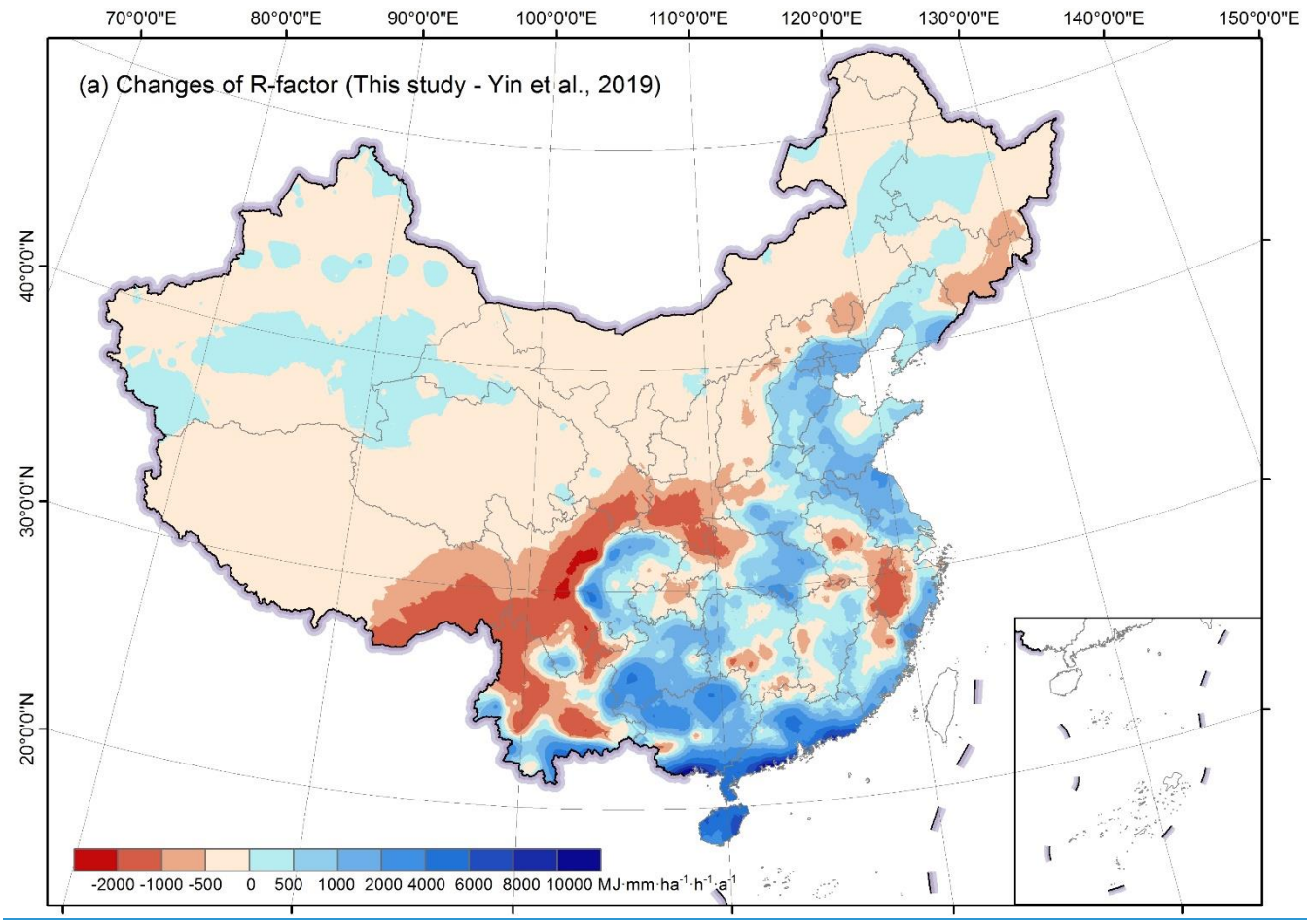
(a) Changes of R-factor (This study - Yin et al., 2019)
70°0'0"E
80°0'0"E
90°0'0"E
100°0'0"E
110°0'0"E
120°0'0"E
130°0'0"E
140°0'0"E
150°0'0"E
40°0'0"N
30°0'0"N
20°0'0"N
-2000 -1000 -500 0 500 1000 2000 4000 6000 8000 10000 MJ·mm·ha-1·h-1·a-1

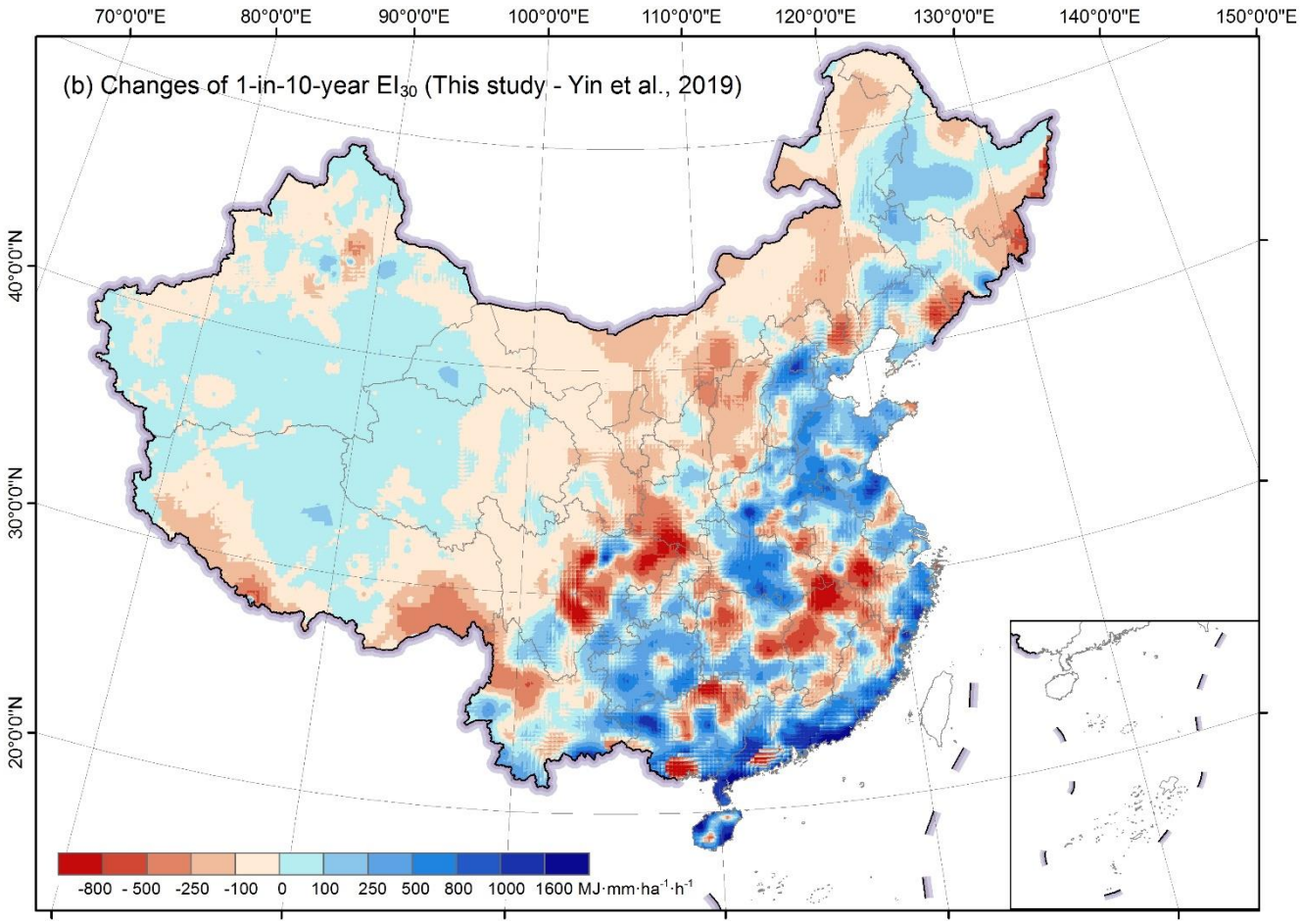

Figure 9: Differences~~Changes~~ of the ~~R factor~~R-factor(a) and the 1-in-10-year EI_{30}(b) comparing with the previous study

Comparing with the maps from Yin et al. (2019), the new maps can be quite different at some local areas (Fig. ~~6a~~ 9a and ~~6b~~9b). The ~~R factor~~R-factor in the new map was higher for most of the southeastern area, and lower for most of the middle and western areas, especially for the southwestern area (Fig. ~~6a~~9a). The~~ change~~ map of 1-in-10-year event EI_{30} demonstrated similar pattern with that of ~~R factor~~R-factor, whereas with more negative values in some eastern mountainous areas (Fig. 9b).

3.3 ~~Contribution analysis on the improvement of erosivity maps~~Evaluation on the improvement of the erosivity maps

3.3.1 ~~Contribution~~ Effect of data temporal resolution

Figure 10 ~~Figure 7~~ shows that the ~~R factor~~R-factor estimated from daily data (Eq. 12) is underestimated when the R value is higher than 10,000 MJ mm ha^{-1} h^{-1} a^{-1}, and slightly overestimated when the value is lower than 2,000 MJ mm ha^{-1} h^{-1} a^{-1}. The model using hourly data improved the accuracy by about 11.1% (median value of the relative error) compared to that from daily data (Fig. 10~~7~~). Estimated 1-in-10-year EI_{30} would be underestimated using hourly and daily data, and the

underestimation is greater if daily data were used (Fig. ~~7~~10). Unlike the ~~R factor~~R-factor, 1-in-10-year EI_{30} was not noticeably improved with an increase in the temporal resolution from daily to hourly data, probably due to the fact that the 1-in-10-year EI_{30} values estimated using daily data in Yin et al. (2019) had already been multiplied by a conversion factor of 1.17 to correct the 1-in-10-year daily erosivity to approximate the true 1-in-10-year EI_{30} from 1-min data.

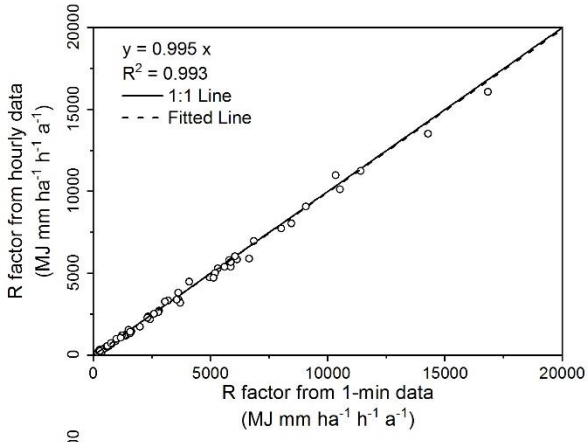
y = 0.995 x
R² = 0.993
1:1 Line
Fitted Line
R factor from hourly data
(MJ mm ha⁻¹ h⁻¹ a⁻¹)
R factor from 1-min data
(MJ mm ha⁻¹ h⁻¹ a⁻¹)
0
5000
10000
15000
20000

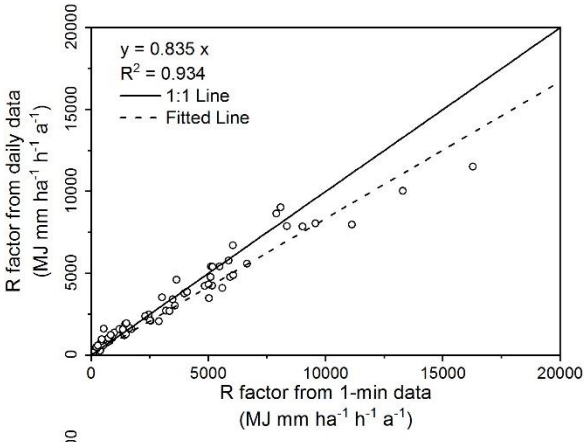
y = 0.835 x
R² = 0.934
1:1 Line
Fitted Line
R factor from daily data
(MJ mm ha⁻¹ h⁻¹ a⁻¹)
R factor from 1-min data
(MJ mm ha⁻¹ h⁻¹ a⁻¹)
0
5000
10000
15000
20000

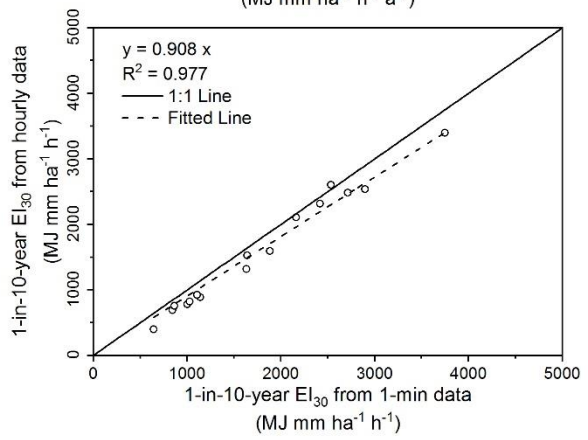
y = 0.908 x
R² = 0.977
1:1 Line
Fitted Line
1-in-10-year EI30 from hourly data
(MJ mm ha⁻¹ h⁻¹)
1-in-10-year EI30 from 1-min data
(MJ mm ha⁻¹ h⁻¹)
0
1000
2000
3000
4000
5000

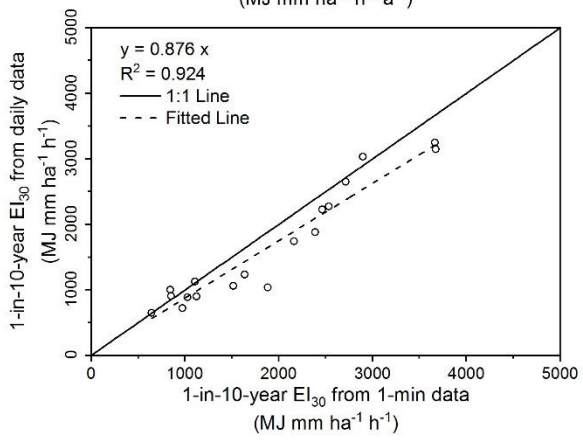
y = 0.876 x
R² = 0.924
1:1 Line
Fitted Line
1-in-10-year EI30 from daily data
(MJ mm ha⁻¹ h⁻¹)
1-in-10-year EI30 from 1-min data
(MJ mm ha⁻¹ h⁻¹)
0
1000
2000
3000
4000
5000

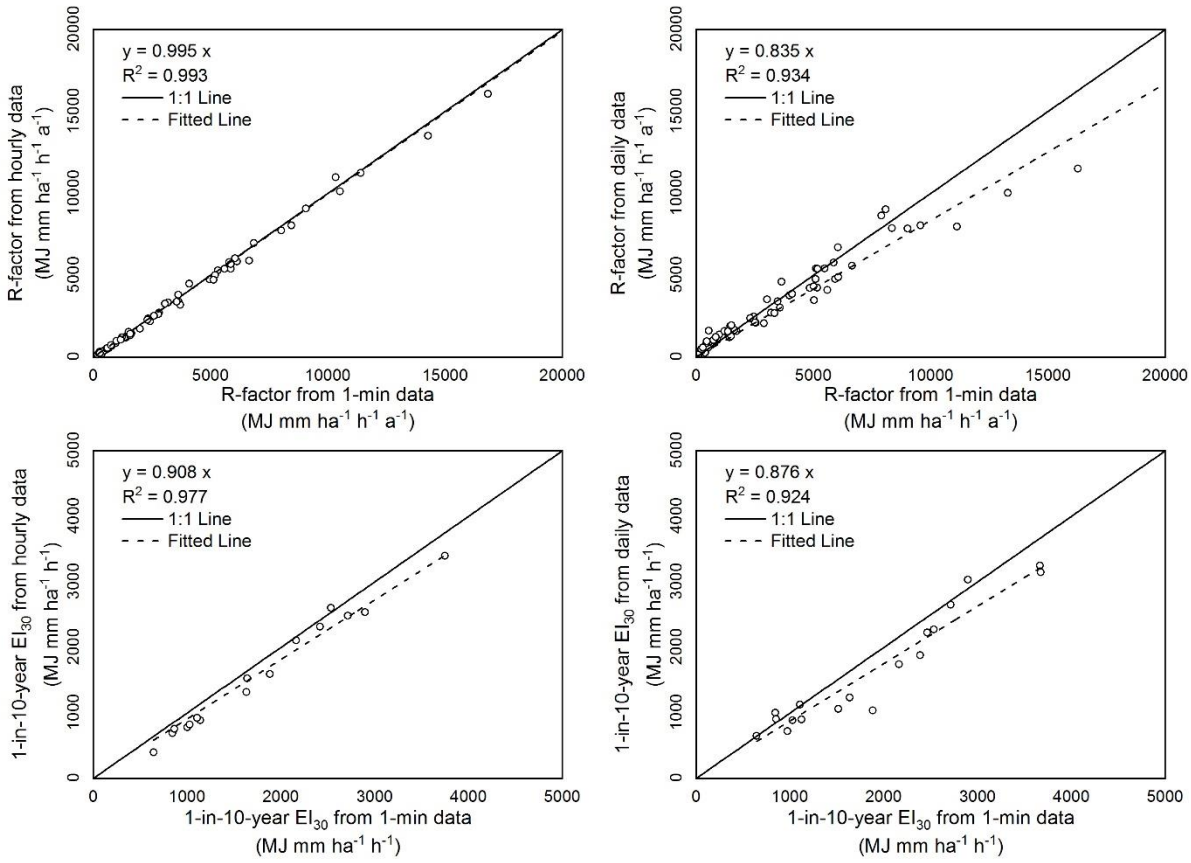

Figure 10: Comparison of the ~~R factor~~R-factor (upper) and 1-in-10-year EI_{30} (lower) estimated from hourly (left) and daily (right) rainfall data

3.3.2 ~~Contribution~~ Effect of the station density

Interpolation for the Western (W) region had the least NSE compared to others, which may be induced by the sparsity of stations (Fig. 1) and the lower spatial correlation of rainfall. The fitted semivariogram for the ~~R factor~~R-factor in W region had a range of 35 km, whereas the ranges for Mid-western (MW), Northeastern (NE) and Southeastern (SE) regions were 288, 261 and 1,235 km, respectively.

A comparison of cross-validation between the two maps with different station densities shows that the interpolation with denser stations can improve the accuracy by 2.6% ~ 15.4% for the ~~R factor~~R-factor based on the sMAPE index, and by 1.4% ~ 31.8% for 1-in-10-year EI_{30} (Table 4~~Table 3~~) when the station density increased. The NSE can increase by 0.016 to 0.109 for ~~R factor~~R-factor. For 10-year EI_{30}, the NSE decreased in region W, MW and SE, and increased by 0.038 in region NE.

For the ~~R factor~~R-factor, in region W, the station density doubled (increased from 36, ~~6~~00 to 21,~~2~~00 ~~10~~³ km² 1 station), and the accuracy improved by 15.4%, whereas the sMAPE of 53.3% was still high with this increase in station density. In region

MW, the station density tripled (from 13,900 to 4,800 ~~10^3~~ km^2 1 station) and the accuracy was improved by 11.1% based on the sMAPE index from 30.7% to 19.6%. In region NE and SE, the station density tripled and quadrupled, respectively, and the accuracy increased about 2.5%. For 1-in-10-year EI_{30}, the improvement for the 1-in-10-year EI_{30} was even more (by 31.8% in region W and 19.6% in region MW). The improvement was mainly in western regions, and the station density in the eastern China before the increase is enough to describe the spatial variation of the ~~R-factor~~R-factor and the 1-in-10-year EI_{30}. It can be inferred that when there were less than about 10,000 ~~10^3~~ km^2 1 station, the increasing of the site density has little impact on the improvement of the interpolation (Fig. ~~8~~11).

Table 4~~Table 3~~: Comparison of cross-validation results for erosivity maps interpolated based on data from 774 and 2381 stations

Region	No. of the stations	Density of the stations (10^3 km^2 1 station)	~~R-factor~~R-factor		1-in-10-year EI_{30}	
			sMAPE	NSE	sMAPE	NSE
W	87	36.6	68.7%	0.489	63.7%	0.389
	150	21.2	53.3%	0.599	31.8%	0.293
MW	161	13.9	30.7%	0.938	44.0%	0.887
	471	4.8	19.6%	0.951	24.5%	0.886
NE	214	11.0	12.4%	0.946	17.0%	0.857
	690	3.4	9.7%	0.962	14.9%	0.895
SE	389	6.6	10.9%	0.942	15.5%	0.844
	1362	1.9	8.3%	0.959	14.0%	0.824

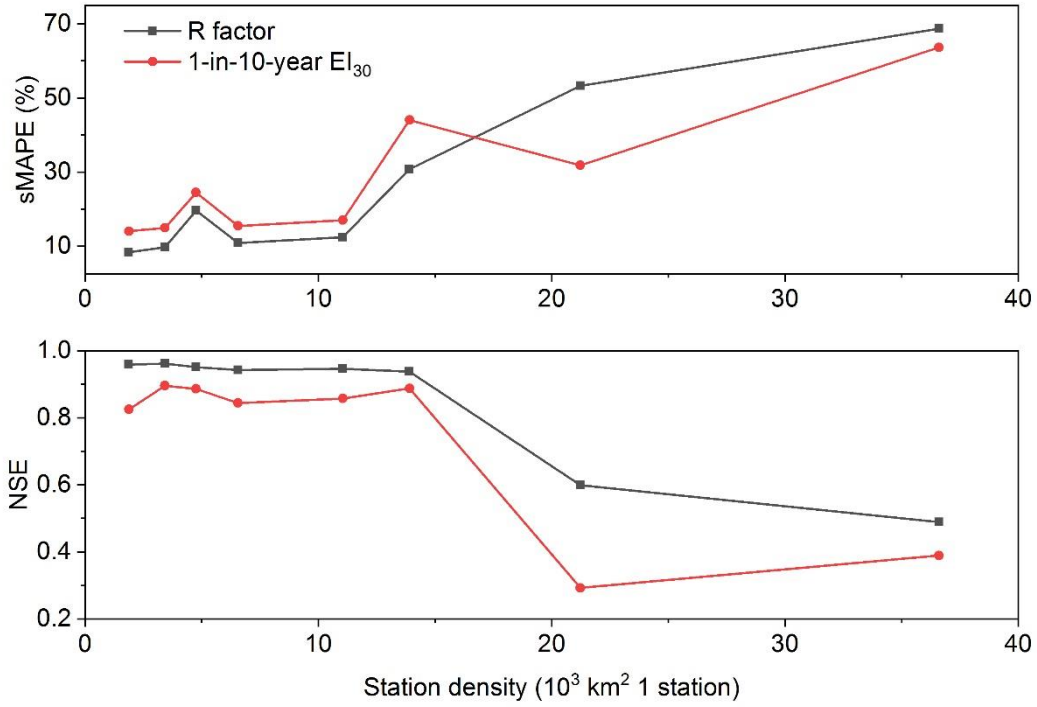
R factor
1-in-10-year EI30
sMAPE (%)
70
50
30
10
0
10
20
30
40
1.0
0.8
0.6
0.4
0.2
NSE
Station density (10^3 km^2 1 station)

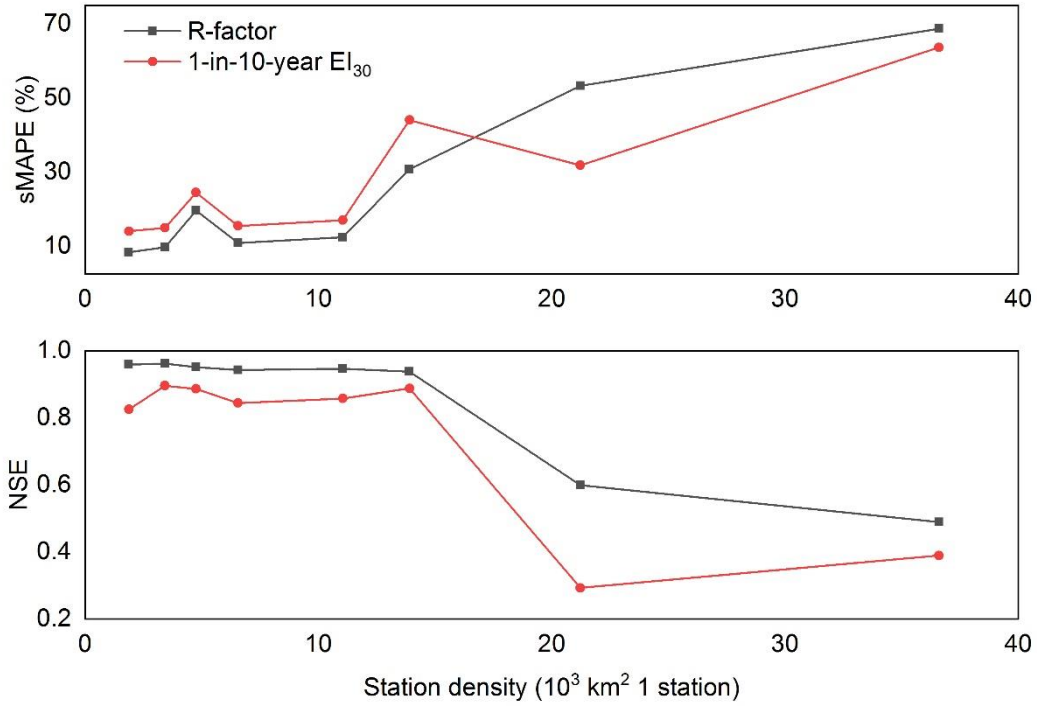
R-factor
1-in-10-year EI30
sMAPE (%)
70
50
30
10
0
10
20
30
40
1.0
0.8
0.6
0.4
0.2
NSE
Station density (10^3 km^2 1 station)

Figure 11: Improvement of the interpolation with the increase of station density. Data were from the 774 and 2381 stations in the 4 different regions

3.3.3 ~~Contribution~~ Effect of the interpolation method

For the ~~R factor~~R-factor, cross-validation of Ordinary Kriging and Universal Kriging with the mean annual rainfall as the co-variable (Table 5~~Table 4~~) shows that UK improved the interpolation accuracy by 2.3%-9.0% (sMAPE) compared to OK. In the western region, the NSE increased from 0.285(OK) to 0.599(UK). Therefore, it is better to use UK instead of OK when generating the ~~R factor~~R-factor map, especially in western China where station density was low. For 1-in-10-year EI_{30}, UK improved the accuracy by 0.4%-9.7% (sMAPE). In region W, the accuracy improved by 9.7% and the NSE increased from 0.094(OK) to 0.293(UK).

Table 5~~Table 4~~: Cross-validation results of interpolation of ~~R factor~~R-factor and 10-year EI_{30} using OK and UK

Region	Interpolation method	~~R factor~~R-factor		1-in-10-year EI_{30}	
		sMAPE	NSE	sMAPE	NSE
W	OK	62.3%	0.285	41.5%	0.094
	UK	53.3%	0.599	31.8%	0.293
MW	OK	24.8%	0.861	24.9%	0.838
	UK	19.6%	0.951	24.5%	0.886
NE	OK	12.0%	0.926	16.5%	0.865
	UK	9.7%	0.962	14.9%	0.895
SE	OK	11.2%	0.911	14.8%	0.844
	UK	8.3%	0.959	14.0%	0.824

4 Discussion

This study produced quality ~~R factor~~R-factor and 1-in-10-year EI_{30} maps with hourly data from 2,381 stations over mainland China. The improvement of the ~~R factor~~R-factor map over previously published ~~R factor~~R-factor map can be contributed to the increase in the temporal resolution from daily to hourly data, whereas that of 1-in-10-year EI_{30} map to the increase of the station density in comparison with those of Yin et al. (2019). There are mainly two reasons for this. First, 1-in-10-year event EI_{30} values estimated from the daily data had already been adjusted to those from the 1-min data by multiplying a conversion factor of 1.17 (Yin et al., 2019) , which resulted in no obvious improvement from the daily data to hourly data. Second, the 1-in-10-year event EI_{30} associated with extreme rainfall event intrinsically has a high spatial variability in comparison to the annual average rainfall erosivity as shown in Table ~~4~~3. The accuracy of spatially interpolated rainfall erosivity was more sensitive to the station density when the station density is low. Hence the improvement of the map of the 1-in-10-year EI_{30} was mainly contributed to the increase of the station density, especially for the western and the mid-western regions with sparse station density.

The uncertainty of the results from this study mainly comes from the following aspects: (a) KE-I model for estimating Kinetic Energy (KE) from the instant precipitation Intensity (I). KE-I model used in this study is from RUSLE2 (USDA-ARS, 2013) and raindrop disdrometer observation data need to be collected to calibrate the KE-I model in future. (b) The estimation of the erosivity factors from hourly data (Eq. (5)). The conversion factors were developed based on 1-min rainfall data from 62 stations (Fig. 2). Hourly data brings information loss in the estimation of instant precipitation intensity comparing with breakpoint data. (c) The adjustment of the R-factor from the stations with less effective years (Eq. (8)). This is based on a power function (Eq. (9)) of the mean annual precipitation and rainfall erosivity using 1-min and daily rainfall data of 35 stations; The degree of uncertainty mainly depends on the ~~annual~~ variation of annual rainfall erosivity. (d) Station distribution and density. In western China, the stations were sparse and unevenly distributed, which affect the interpolation accuracy. (e) Spatial interpolation model (Universal Kriging in this study) and the interpolation procedures (the division of regions before the interpolation and the mergence of regions after the interpolation).

Panagos et al. (2017) developed a Global Rainfall Erosivity Database with hourly and sub-hourly rainfall data from 3,625 stations over 63 countries, ~~for water erosion assessment for many regions of the world especially where observational data were limited~~which ~~,~~ has provided a good basis for the comparison of rainfall erosivity among different regions in the world. In their study, rainfall data at 60-min interval from 387 stations across China were used. Figure 12 ~~Figure 9~~ shows that the ~~R factor~~R-factor for China extracted from Panagos et al. (2017) is systematically underestimated by about 30% for most areas in China, whereas overestimated in the Tibetan Plateau (cf. Fig. ~~5a~~7a). The reason for the underestimation may be that the ~~R factor~~R-factor calculated from 60-min interval data applied a conversion factor (CF_{30}) that was developed from the values estimated by 60-min data to those by 30-min data in Panagos et al. (2015), rather than a factor to those by breakpoint data (CF_{bp}) or 1-min data (CF_1), which were used in USLE (Wischmeier and Smith, 1965, 1978), RUSLE (Renard, 1997) and this study. Previous research have showed the difference between CF_{30} and CF_{bp} (CF_1) can result in an underestimation of ~~R factor~~R-factor by about 20% (Auerswald et al., 2015; Yue et al., 2020). ~~Table 5~~Table 6 shows that the relative error of the map from Panagos et al. (2017) could reduce by about 6.2% after multiplying by a conversion factor of 1.253, which was calibrated by Yue et al. (2020) for converting the ~~R factor~~R-factor from 30-min data to 1-min data (Because the cross-validation values from the map of Panagos et al. (2017) were not available, the values extracted from the maps were instead to compare with the true values from 1-min data at the 62 stations). The adjusted map still generally underestimated. The reason may be that the equation for estimating the storm energy (E) used in Panagos et al. (2017) was from RUSLE (Renard, 1997), which have been reported an underestimation of the storm energy up to 10% in previous studies (McGregor et al., 1995; Yin et al., 2017). Because of this, the equation for estimating the storm energy (E) in RUSLE (Renard, 1997) was then modified in RUSLE2 (USDA-ARS, 2013), which was adopted in this study.

The ~~R factor~~R-factor in the Tibetan Plateau varies from 0 to 12,326 MJ mm ha^{-1} h^{-1} a^{-1} in Panagos et al. (2017), and from 5~~4.6~~ to 4,44~~21.9~~ MJ mm ha^{-1} h^{-1} a^{-1} in this study. The former was derived from a Gaussian Process Regression (GPR) model and a number of monthly climate variables from the WorldClim database, such as the mean monthly precipitation, mean minimum, average and maximum monthly temperature. The GPR model was calibrated using the site-specific ~~R factor~~R-factor values

and these climate variables, which may not applicable for sites at high altitude, as none of the observation sites was located in the Tibetan Plateau region. The GPR model might be the main reason for the overestimation of the ~~R factor~~R-factor in the Tibetan Plateau where the ~~R factor~~R-factor was expected to be underestimated just like any other regions.

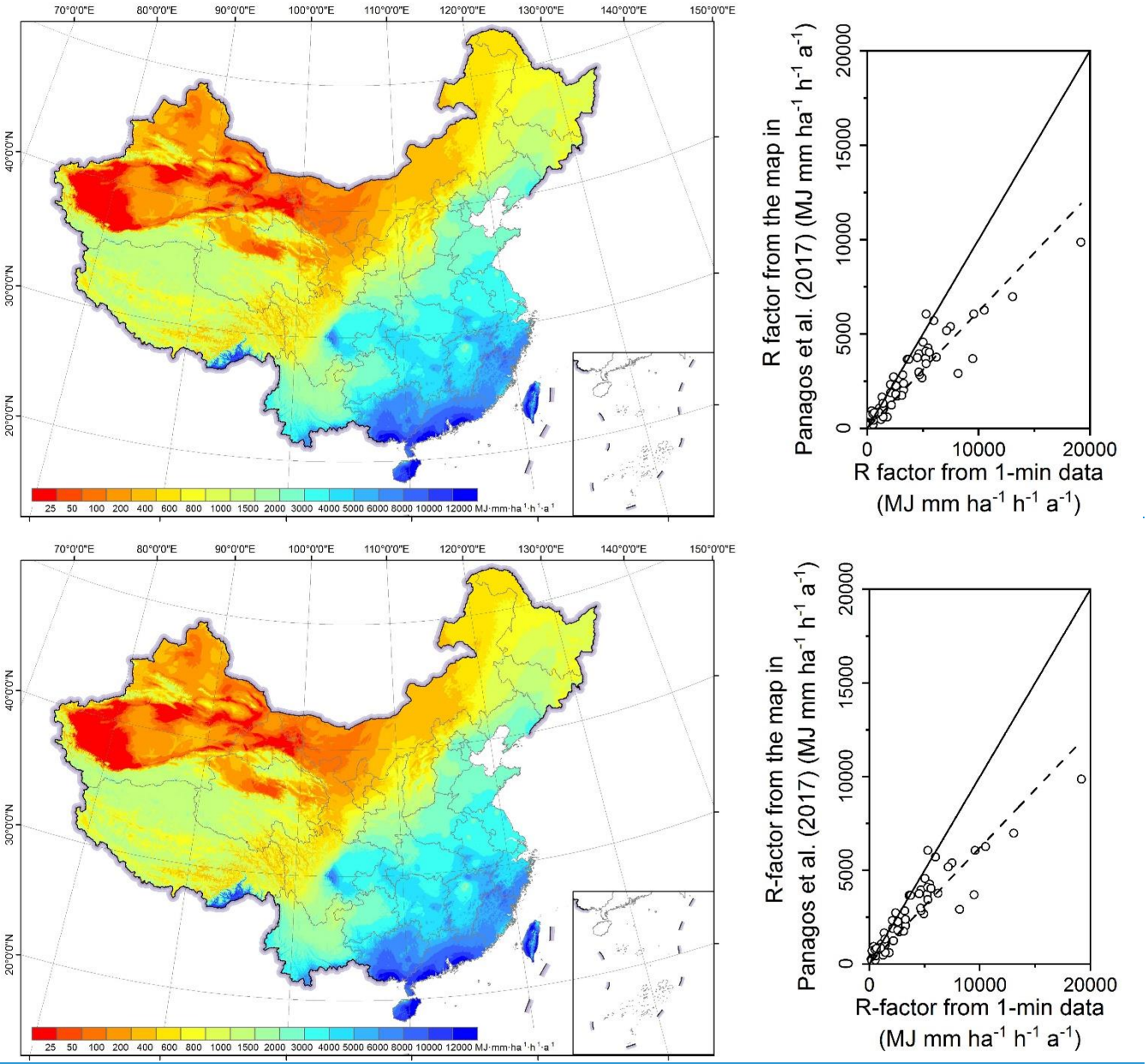

Figure 12: ~~R factor~~R-factor map for China extracted from Panagos et al. (2017) and the evaluation of the map based on 62 stations with 1-min data.

Table 6~~Table 5~~: Comparison of the statistical characteristics of the relative errors of the ~~R factor~~R-factor extracted from the map~~s~~ generated in this study and extracted from Panagos et al. (2017) (original and adjusted). The adjusted map of Panagos et al. (2017) was the original map multiplying by a conversion factors of 1.253, which was calibrated by Yue et al. (2020) for converting the ~~R factor~~R-factor from 30-min data to 1-min data.

	This study	Panagos et al. (2017)	Panagos et al. (2017) adjusted
25th percentile	7.1%	14.8%	10.4%
Median	16.1%	28.3%	22.1%
75th percentile	28.0%	40.5%	43.2%
Mean	20.1%	33.8%	33.1%

5 Conclusions

This study generated the ~~R factor~~R-factor and 1-in-10-year EI_{30} maps using hourly and daily rainfall data for the period from 1951 to 2018 from 2,381 stations over mainland China. The improvement in the accuracy of these erosivity maps was evaluated against the current maps (maps from Yin et al. (2019) were taken as references) in terms of temporal resolution of the rainfall data, the station density, and the interpolation method. The conclusions were drawn as follows:

(1) Comparing with the current maps for the 62 reference sites, the ~~R factor~~R-factor map generated in this study improved the accuracy from 1~~9.4~~8.1% to 1~~5.9~~7.8% in the mid-western and eastern regions, ~~45.2~~161.6% to ~~21.6~~16.2% in the western region, and the 1-in-10-year EI_{30} map improved the accuracy from ~~21.7~~20.6% to 13.~~05~~% in the mid-western and eastern regions.

(2) The ~~R factor~~R-factor and the 1-in-10-year EI_{30} increased from the northwestern to the southeastern China. The ~~R factor~~R-factor was from 0 to 25,300 MJ mm ha^{-1} h^{-1} a^{-1}, and the 1-in-10-year EI_{30} was from 0 to 11,246 MJ mm ha^{-1} h^{-1}. Comparing with the current maps, the ~~R factor~~R-factor and 1-in-10-year event EI_{30} in the new maps were higher for most of the southeastern area, and lower for most of the middle and western areas.

(3) The improvement of the ~~R factor~~R-factor map can be mainly contributed to the increase of the temporal resolution from daily to hourly, whereas that of 1-in-10-year EI_{30} map to the increase of station density. The increased station density mainly improved the accuracy in the western regions for both the ~~R factor~~R-factor and 1-in-10-year EI_{30}. ~~T~~The benefit of an increased ~~he contribution of increasing the~~ station density is limited~~to improve the interpolation was limited~~ once ~~when~~ the station density reached 1 station per 10,000 km^2.~~was denser than about 10,000 10^3 km^2 1 station.~~ As for the interpolation method, Universal Kriging with the mean annual rainfall as the co-variable performed better than Ordinary Kriging for all regions, especially for the western regions.

Data availability

The Rainfall erosivity maps (~~R factor~~R-factor and 1-in-10-year EI_{30}) are available at: https://dx.doi.org/10.12275/bnu.clicia.rainfallerosivity.CN.001 (Yue et al., 2020)

Competing interests

The authors declare that they have no conflict of interest.

Acknowledgments

This work was supported by National Key R&D Program (no.2018YFC0507006) and the National Natural Science Foundation of China (no. 41877068). We also would like to thank the high-performance computing support from the Center for Geodata and Analysis, Faculty of Geographical Science, Beijing Normal University [https://gda.bnu.edu.cn/]

References

Alewell, C., Borelli, P., Meusburger, K. and Panagos, P.: Using the USLE: Chances, challenges and limitations of soil erosion modelling, Int. soil water Conserv. Res., 7(3), 203–225, doi:10.1016/j.iswcr.2019.05.004, 2019.

Angulomart ínez, M. and Beguer á, S.: Estimating rainfall erosivity from daily precipitation records: a comparison among methods using data from the Ebro Basin (NE Spain), J. Hydrol., 379(1–2), 111–121, 2009.

Arnoldus, H. M. J.: Methodology used to determine the maximum potential average annual soil loss due to sheet and rill erosion in Morocco, FAO Soils Bull., 1977.

Auerswald, K., Fiener, P., Gomez, J. A., Govers, G., Quinton, J. N. and Strauss, P.: Comment on "Rainfall erosivity in Europe" by Panagos et al.(Sci. Total Environ., 511, 801–814, 2015), Sci. Total Environ., 532, 849–852, 2015.

Bagarello, V. and D'Asaro, F.: Estimating single storm erosion index, Trans. ASAE, 37(3), 785–791, 1994.

Bonilla, C. A. and Vidal, K. L.: Rainfall erosivity in central Chile, J. Hydrol., 410(1–2), 126–133, 2011.

Borrelli, P., Diodato, N. and Panagos, P.: Rainfall erosivity in Italy: a national scale spatiotemporal assessment, Int. J. Digit. Earth, 2016.

Capolongo, D., Diodato, N., Mannaerts, Cm., Piccarreta, M. and Strobl, R. O.: Analyzing temporal changes in climate erosivity using a simplified rainfall erosivity model in Basilicata (southern Italy), J. Hydrol., 356(1–2), 119–130, 2008.

Coles, S. G.: An introduction to statistical modeling of extreme values. - springer, 2001.

FAO: Outcome document of the Global Symposium on Soil Erosion, Rome. [online] Available from: http://www.fao.org/3/ca5697en/ca5697en.pdf, 2019a.

FAO: Soil erosion: the greatest challenge to sustainable soil management, Rome. [online] Available from: http://www.fao.org/3/ca4395en/ca4395en.pdf, 2019b.

Ferrari, R., Pasqui, M., Bottai, L., Esposito, S. and Di Giuseppe, E.: Assessment of soil erosion estimate based on a high temporal resolution rainfall dataset, in Proc. 7th European Conference on Applications of Meteorology (ECAM), Utrecht, Netherlands, pp. 12–16., 2005.

Ferro, V., Giordano, G. and Iovino, M.: Isoerosivity and erosion risk map for Sicily, Hydrol. Sci. J., 36(6), 549–564, 1991.

Haith, D. A. and Merrill, D. E.: Evaluation of a daily rainfall erosivity model, Trans. ASAE, 30(1), 90–93, 1987.

Hosking, J. R. M.: L-Moments: Analysis and Estimation of Distributions Using Linear Combinations of Order Statistics, J. R. Stat. Soc., 52(1), 105–124, 1990.

Klik, A., Haas, K., Dvorackova, A. and Fuller, I. C.: Spatial and temporal distribution of rainfall erosivity in New Zealand, Soil Res., 40(6), 887–901, 2015.

Lee, J.-H. and Heo, J.-H.: Evaluation of estimation methods for rainfall erosivity based on annual precipitation in Korea, J. Hydrol., 409(1–2), 30–48, 2011.

Liu, B., Tao, H. and Song, C.: Temporal and spatial variations of rainfall erosivity in China during 1960 to 2009, Geogr. Res., 32(2), 245–256, 2013.

Liu, Y., Zhao, W., Liu, Y. and Pereira, P.: Global rainfall erosivity changes between 1980 and 2017 based on an erosivity model using daily precipitation data, Catena, 194, 104768, 2020.

Lu, H. and Yu, B.: Spatial and seasonal distribution of rainfall erosivity in Australia, Soil Res., 40(6), 887–901, 2002.

McGregor, K. C., Bingner, R. L., Bowie, A. J. and Foster, G. R.: Erosivity index values for northern Mississippi, Trans. ASAE, 38(4), 1039–1047, 1995.

Naipal, V., Reick, C. H., Pongratz, J. and Van Oost, K.: Improving the global applicability of the RUSLE model-adjustment of the topographical and rainfall erosivity factors, Geosci. Model Dev., 8, 2893–2913, 2015.

Oliveira, P. T. S., Rodrigues, D. B. B., Sobrinho, T. A., Carvalho, D. F. De and Panachuki, E.: Spatial variability of the rainfall erosive potential in the State of Mato Grosso do Sul, Brazil, Eng. Agrícola, 32(1), 69–79, 2012.

Panagos, P., Ballabio, C., Borrelli, P., Meusburger, K., Klik, A., Rousseva, S., Tadić, M. P., Michaelides, S. and Hrabalíková, M.: Rainfall erosivity in Europe, Sci. Total Environ., 511, 801–814, 2015.

Panagos, P., Ballabio, C., Borrelli, P. and Meusburger, K.: Spatio-temporal analysis of rainfall erosivity and erosivity density in Greece, Catena, 137, 161–172, 2016.

Panagos, P., Borrelli, P., Meusburger, K., Yu, B., Klik, A., Lim, K. J., Yang, J. E., Ni, J., Miao, C. and Chattopadhyay, N.: Global rainfall erosivity assessment based on high-temporal resolution rainfall records, Sci. Rep., 7(1), 4175, 2017.

Porto, P.: Exploring the effect of different time resolutions to calculate the rainfall erosivity factorRin Calabria, southern Italy, Hydrol. Process., 30(10), 1551–1562, doi:10.1002/hyp.10737, 2016.

Qin, W., Guo, Q., Zuo, C., Shan, Z., Ma, L. and Sun, G.: Spatial distribution and temporal trends of rainfall erosivity in mainland China for 1951–2010, Catena, 147, 177–186, 2016.

Ramos, M. C. and Durán, B.: Assessment of rainfall erosivity and its spatial and temporal variabilities: Case study of the Penedès area (NE Spain), Catena, 123, 135–147, 2014.

Renard, K. G.: Predicting soil erosion by water: a guide to conservation planning with the Revised Universal Soil Loss Equation (RUSLE), United States Government Printing., 1997.

Renard, K. G. and Freimund, J. R.: Using monthly precipitation data to estimate the R-factor in the revised USLE, 1994.

Richardson, C. W., Foster, G. R. and Wright, D. A.: Estimation of erosion index from daily rainfall amount, Trans. ASAE, 26(1), 153–156, 1983.

Riquetti, N. B., Beskow, S. and Viola, M. R.: Rainfall erosivity in South America: Current patterns and future perspectives, Sci. Total Environ., 724, 138315, doi:10.1016/j.scitotenv.2020.138315, 2020.

Sadeghi, S. H., Zabihi, M., Vafakhah, M. and Hazbavi, Z.: Spatiotemporal mapping of rainfall erosivity index for different return periods in Iran, Nat. Hazards, 87(1), 35–56, 2017.

Selker, J. S., Haith, D. A. and Reynolds, J. E.: Calibration and testing of a daily rainfall erosivity model, , 33(5), 1612, 1990.

Sheridan, J. M., Davis, F. M., Hester, M. L. and Knisel, W. G.: Seasonal distribution of rainfall erosivity in peninsular Florida, Trans. ASAE, 32(5), 1555–1560, 1989.

Silva, R. M., Santos, C., Silva, J., Silva, A. M. and Neto, R.: Spatial distribution and estimation of rainfall trends and erosivity in the Epitácio Pessoa reservoir catchment, Paraíba, Brazil, Nat. Hazards J. Int. Soc. Prev. Mitig. Nat. Hazards, 102, doi:10.1007/s11069-020-03926-9, 2020.

Tao, L. I., Zheng, X., Dai, Y., Yang, C., Chen, Z., Zhang, S. and Guocan, W. U.: Mapping Near-surface Air Temperature, Pressure, Relative Humidity and Wind Speed over Mainland China with High Spatiotemporal Resolution, Adv. Atmos. Sci., 031(5), 1127–1135, 2014.

USDA-ARS: Science documentation: Revised Universal Soil Loss Equation Version 2 (RUSLE2), USDA-Agricultural Research Service, Washington, D.C., 2013.

Wang, W., Jiao, J., Hao, X., Zhang，Xiankui and Lu, X.: Distribution of rainfall erosivity R value in China, J. Soil Eros. Soil Conserv., (1), 1, 1996.

Wischmeier, W. H.: A Rainfall Erosion Index for a Universal Soil-Loss Equation 1, Proc Soil Sci. Soc. Am., 23(3), 246–249, 1959.

Wischmeier, W. H. and Smith, D. D.: Rainfall energy and its relationship to soil loss, Trans.am.gephys.union, 39(2), 285–291, 1958.

Wischmeier, W. H. and Smith, D. D.: Predicting rainfall-erosion losses from cropland east of the Rocky Mountains: Guide for selection of practices for soil and water conservation, US Department of Agriculture., 1965.

Wischmeier, W. H. and Smith, D. D.: Predicting rainfall erosion losses: a guide to conservation planning, Department of Agriculture, Science and Education Administration., 1978.

Xie, Y., Liu, B. Y. and Zhang, W. B.: Study on standard of erosive rainfall, J. soil water Conserv., 14(4), 6–11, 2000.

Xie, Y., Yin, S. Q., Liu, B. Y., Nearing, M. A. and Zhao, Y.: Models for estimating daily rainfall erosivity in China, J. Hydrol., 535, 547–558, 2016.

Yang, X. and Yu, B.: Modelling and mapping rainfall erosivity in New South Wales, Australia, Soil Res., 53(2), 178–189, 2015.

Yin, S., Xie, Y., Liu, B. and Nearing, M. A.: Rainfall erosivity estimation based on rainfall data collected over a range of temporal resolutions., Hydrol. Earth Syst. Sci. Discuss., 12(5), 2015.

Yin, S., Nearing, M. A., Borrelli, P. and Xue, X.: Rainfall Erosivity: An Overview of Methodologies and Applications, Vadose Zo. J., 16(12), 2017.

Yin, S., Xue, X., Yue, T., Xie, Y. and Gao, G.: Spatiotemporal distribution and return period of rainfall erosivity in China(in Chinese), Trans. Chinese Soc. Agric. Eng., 2019.

Yu, B. and Rosewell, C. J.: Rainfall erosivity estimation using daily rainfall amounts for South Australia, Soil Res., 34(5), 721–733, 1996a.

Yu, B. and Rosewell, C. J.: Technical notes: a robust estimator of the R-factor for the universal soil loss equation, Trans. ASAE, 39(2), 559–561, 1996b.

Yu, B., Rosewell, C. J., Yu, B. and Rosewell, C. J.: An assessment of a daily rainfall erosivity model for New South Wales, Aust. J. Soil Res., 34(1), 139–152, 1996.

Yue, T., Xie, Y., Yin, S., Yu, B., Miao, C. and Wang, W.: Effect of time resolution of rainfall measurements on the erosivity factor in the USLE in China, Int. soil water Conserv. Res., doi:https://doi.org/10.1016/j.iswcr.2020.06.001, 2020.

Zhang, W., Xie, Y. and Liu, B.: Spatial distribution of rainfall erosivity in China, J. Mt. ence, 21(1), 33–40, 2003.

Zhang, W. B., Xie, Y. and Liu, B. Y.: Rainfall Erosivity Estimation Using Daily Rainfall Amounts, Sci. Geogr. Sin., (6), 53–56, 2002.

Zhu, Z. and Yu, B.: Validation of Rainfall Erosivity Estimators for Mainland China, Trans. ASABE, 58(1), 61–71, 2015.